Particle Filter Based Target Tracking from X-band Nautical Radar Images

by

©Supeng Chen, B.Eng., M.Eng.

A thesis submitted to the School of Graduate Studies in partial fulfillment of the requirements for the degree of

Master of Engineering

Faculty of Engineering and Applied Science

Memorial University of Newfoundland

May 2014

St. John's Newfoundland

Abstract

In this thesis, two particle filter (PF) based visual tracking approaches are designed for maneuvering target tracking from X-band nautical radar images: a PF-only based approach and a combined particle-Kalman filters (PF-KF) based approach. Unlike existing Kalman filter (KF) based target tracking algorithms used by nautical radar, these two proposed tracking methods both employ a kernel-based histogram model to represent the target in the radar image, and a Bhattacharyya coefficient based similarity distance between reference and candidate target models to provide the likelihood function for the particle filtering. However, the PF-KF method applies a sampling importance resampling (SIR) particle filter to obtain preliminary target positions, and then a Kalman filter to derive refined target positions and velocities. Moreover, several strategies are also proposed to improve the tracking accuracy and stability. These strategies include an enhanced reference target model construction method, updating reference target model, and adaptive KF for maneuver. Comparison of the target information obtained by the proposed PF-KF method from various field X-band nautical radar image sequences with those measured by GPS shows the proposed approach can provide a reliable and flexible online target tracking for nautical radar application. It is also shown that, in the scenario of strong sea clutter, the proposed approach outperforms the PF-only based approach and the classical tracking approach which combines order-statistics (OS) CFAR processing and the Kalman filter.

Acknowledgements

The author would like to thank Dr. Weimin Huang and the Faculty of Engineering and Applied Science for providing him the excellent opportunity of research at Memorial University of Newfoundland. Particularly, the author is really grateful for the earnest supervision of Dr. Huang and his valuable suggestions and encouragement throughout the research and living here.

The author would also like to thank the members in the radar group, in particular Dr. Eric Gill, Jiaqi An, Chen Li, Chengxi Shen, and Khalid El-Darymli, for their ardent and inspiring help to this work.

The author would like to thank the financial support from the Research and Development Corporation (RDC) IRIF Ignite grant (207765) and a Natural Sciences and Engineering Research Council of Canada Discovery Grant (NSERC 402313-2012) to Dr. W. Huang, and the Rutter Inc. for providing the radar and GPS data.

Finally, the author is sincerely grateful for the support and sacrifice of the author's family, especially his wife and his father. Without them, this work would not have been completed.

Table of Contents

List of Tables

List of Figures

Table of Symbols

P_{fa} Probability of false alarm (p. 12).

P_d Probability of detection (p. 12).

X Pixel intensity of the radar image (p. 12).

X_T Intensity threshold for target detection (p. 12).

x_k^m Measured x coordinate of the target center in the Cartesian radar image at time k (p. 13).

y_k^m Measured y coordinate of the target center in the Cartesian radar image at time k (p. 13).

$h_i^{k,t}$ Intensity of a target signal in the radar image at time k (p. 13).

x_k^s Smoothed target position at time k (p. 14).

x_k^p Predicted target position at time k (p. 14).

$\dot{x}_k^s$ Smoothed target velocity at time k (p. 14).

α The α coefficient of the α-β filter (p. 14).

β The β coefficient of the α-β filter (p. 14).

T Interval between successive radar scans (p. 14).

$\boldsymbol{s}_k$ State vector at time k for the dynamic tracking system (p. 14).

$\boldsymbol{z}_k$ Target measurement at time k for the dynamic tracking system (p. 14).

$\boldsymbol{u}_k$ Process noise at time k for the dynamic tracking system (p. 14).

$\boldsymbol{v}_k$ Measurement noise at time k for the dynamic tracking system (p. 14).

$\boldsymbol{f}_k(\cdot)$ State transition function of the dynamic tracking system (p. 14).

$\boldsymbol{h}_k(\cdot)$ Measurement function of the dynamic tracking system (p. 14).

$\boldsymbol{F}_k$ Linear state transition function at time k for the dynamic tracking system (p. 15).

$\boldsymbol{H}_k$ Measurement function at time k for the dynamic tracking system (p. 15).

$\boldsymbol{Q}_k$ Covariance matrix of the process noise at time k (p. 15).

$\boldsymbol{R}_k$ Covariance matrix of the measurement noise at time k (p. 15).

$\boldsymbol{K}_k$ Kalman gain at time k in the Kalman filter (p. 15).

$\boldsymbol{P}_{k|k-1}$ Estimation error at time k before the measurement is updated in the Kalman filter (p. 15).

$a_{x,k}$ Acceleration along the x-axis of the Cartesian radar image at time k (p. 16).

$a_{y,k}$ Acceleration along the y-axis of the Cartesian radar image at time k (p. 16).

$\boldsymbol{\nu}_k$ Innovation term at time k in the Kalman filter (p. 17).

$\boldsymbol{\Theta}_k$ Covariance of the innovation term at time k in the Kalman filter (p. 18).

δ_k Normalized squared residual of the innovation term at time k in the Kalman filter (p. 18).

g_k Fading memory average of δ_k (p. 18).

Δ Effective window length of the fading memory for adaptive KF filtering (p. 18).

ρ_w Coefficient to determine the effective window length of the fading memory (p. 18).

$p(\boldsymbol{s}_k\|\boldsymbol{z}_{0:k})$	Conditional posterior probability density function (PDF) on a sequence of consecutive updating observations $\boldsymbol{z}_{0:k}$ (p. 23).
N_s	Number of the samples of particle filtering (p. 23).
$\{\boldsymbol{s}_k^i, w_k^i\}_{i=1}^{N_s}$	One set of discrete random samples with the state vector $\boldsymbol{s}_k^i$ and associated weight w_k^i at time k (p. 23).
$p(\boldsymbol{z}_k\|\boldsymbol{s}_k^i)$	The likelihood function for particle filtering (p. 24).
$q(\cdot)$	The importance density for particle filtering (p. 24).
$p(\boldsymbol{s}_k\|\boldsymbol{s}_{k-1}^i)$	The prior density for particle filtering (p. 24).
$\hat{\boldsymbol{p}}$	Normalized histogram of a candidate target (p. 26).
$\hat{\boldsymbol{q}}$	Normalized histogram of a reference target (p. 26).
$\rho[\hat{\boldsymbol{p}}, \hat{\boldsymbol{q}}]$	Bhattacharyya coefficient of reference and candidate target models (p. 26).
$D(\hat{\boldsymbol{p}}, \hat{\boldsymbol{q}})$	The Bhattacharyya coefficient based distance between reference and candidate target models (p. 26).
B	Number of bins of target histogram model (p. 26).
$k(\cdot)$	Kernel function for target model construction (p. 27).
$\boldsymbol{l}$	Target position within the target region for the target model construction (p. 27).
α_r	Adaptivity coefficient for the reference target model update (p. 32).
$\boldsymbol{s}_k^{\mathrm{PF}}$	State vector for particle filtering in the PF-KF procedure (p. 37).
d	Great-circle distance between two points on the earth (p. 43).
c	Angular distance in radian between two points on the earth (p. 43).
a	Square of half the chord length between two points on the earth (p. 43).
R	Radius of the earth (p. 43).
θ	Bearing between two points on earth (p. 44).

Chapter 1

Introduction

1.1 Background of Study

Target tracking is a process to extract the kinematic information of targets (e.g. target position, velocity or acceleration) from the data collected by various sensors, such as radar, infrared sensors, and optical devices. Automatic target tracking is important for both civilian and military applications. The most typical civilian applications include air traffic control (ATC) and maritime navigation, while military applications include air defense, fire control and interceptor guidance [1].

Target tracking plays an especially important role in nautical applications, such as sea surface ship tracking, iceberg tracking [2], trajectory planning [3], search and rescue [4], and autonomous marine craft navigation [5]. Around busy harbors or traffic lines, target tracking can provide essential information for the vessel traffic service (VTS) to manage the traffic and avoid collisions [3]. In the vessel traffic service zones of the Canadian Pacific region, Canada's Marine Communications and Traffic Services (MCTS) has deployed multiple shore based radars to track vessels [6]. In military applications, the identification and tracking of a friendly or hostile target

is critical for maritime border control [7].

Sensors, such as X-band nautical radar, high-frequency (HF) radar, and the global navigation satellite system (GNSS), have been used for target tracking for nautical applications. HF (3-30 MHz) radar has a long coverage range (more than 200 kilometers), but it is difficult to be installed due to large antennas [8, 9]. GNSS-based target tracking only requires a GNSS signal receiver, but it has relatively low tracking accuracy due to its low resolution [10]. X-band nautical radar (working in 8-12 GHz) has widely been used for ship navigation and weather avoidance [9]. It can be easily installed on ships of various sizes since its antenna is small. The X-band nautical radar can also provide accurate and real-time detection and tracking of sea surface small targets with higher resolution (e.g. general range resolutions: 5 m for X-band radars, 1 km for HF radars, 5 km for the GNSS-R).

Although X-band radar has been accepted as a useful tool for sea surface targets tracking, it is still found challenging due to various factors such as noise, clutter and interference. In this thesis, different algorithms for target tracking from X-band nautical radar images are investigated to improve the tracking performance of a maneuvering target under different levels of sea clutter.

1.2 Literature Review

In classical X-band nautical radar applications, target tracking is usually performed through target detection from temporal radar images [1]. The target is detected using detection techniques such as the constant false alarm rate (CFAR) method [9], time-frequency (TF) analysis technique [11] or neural network processing [12]. As the classical detection algorithm, the CFAR detector, which sets the threshold adaptively based on local image information to realize a constant rate of false detection, has been

studied thoroughly and adopted widely in various practical radar systems due to its effectiveness and simplicity. Different CFAR schemes, such as cell-averaging (CA) CFAR, order-statistics (OS) CFAR, trimmed-mean (TM) CFAR, and log-t CFAR, can be used under different clutter environments [13, 14]. However, it is difficult to maintain constant performance by one CFAR scheme as the sea clutter may not follow any assumed single distribution (e.g. Rayleigh, Weibull, Lognormal, K distributions) under all conditions [15]. The TF technique typically employs various time-frequency transforms (e.g. Fourier and chirplet transforms) to provide additional insights into the radar signals. This technique can improve the performance of moving targets detection, especially for the HF over-the-horizon radar (OTH) radar [16–18]. However, the disadvantage of this technique is that it cannot work well for the detection of a low-speed small target [19]. The neural network (NN) technique, inspired by the animal nervous system, has experienced great research development since the introduction of the back propagation algorithm by Rumelhart in 1986 [20] [21]. Different NN architectures (e.g. multilayer perceptrons (MPL), radial basis function (RBF), convolutional neural networks (CNN)) have been studied for sea-surface target detection due to their good performance for nonlinear signal processing [22–24]. However, their application to target detection under varying and complicated environments is still limited since the algorithm requires pre-training using a large amount of data collected under different scenarios.

The scheme for target tracking is to employ a tracking filter based on the measurements obtained from target detection. The underlying mathematical principle of target tracking can be considered as an estimation and filtering problem of a dynamic tracking system in modern system theory [25]. The tracking filter processes the target measurements to extract the target's kinematic information, reduce the radar measurement error, and predict next target state. Typical tracking filters include fixed-

coefficient filters (e.g. α-β filter), the Kalman filter [26], and the extended Kalman filter (EKF) [27] (or unscented Kalman filter (UKF) [28]) for nonlinear filtering [1,29]. Although the fixed-coefficient α-β filter is still being used in some ATC tracking systems for its simplicity, it does not work well for maneuvering target tracking as it assuming the target is moving with constant speed and constant scan interval [30]. The Kalman filter is optimal for a dynamic system with linear functions and Gaussian-distributed noise, which has wide applications in radar tracking systems. The EKF or UKF is widely used when the dynamic system is nonlinear or non-Gaussian. However, these KF-related filters may not adequately obtain accurate estimation if the linearity of the system functions is weak or the noise distributions are significantly different from the Gaussian distribution [31]. Among nonlinear filters, the particle filter (PF), a sequential Monte Carlo method to recursively estimate the system state [32], works particularly well. It has been successfully applied to target detection and tracking with radar applications [33] or computer vision applications [34]. The PF employs the principle of importance sampling to approximate probability densities by using a set of random samples (or particles) with associated weights, and it is theoretically superior to the EKF or UKF in approximation accuracy but with high computational cost.

In 1993, Gordon [32] proposed the novel particle filter (called Bootstrap filter) approach for nonlinear/non-Gaussian Bayesian state estimation. In [31], a comprehensive study of different particle filters (e.g. the sampling importance resampling (SIR) filter, the auxiliary sampling importance resampling (ASIR) filter, and regularized particle filter (RPF)) and other optimal and suboptimal algorithms, such as the KF, EKF, and approximate grid-based methods, are provided [35–38]. Gustafsson [33] introduced the application of the particle filter for target positioning and tracking in various applications, such as car positioning, integrated navigation sys-

tems, and target tracking for ATC and collision avoidance. Furthermore, the PF can be combined with other tracking algorithms. For example, it can be integrated with the widely used mean-shift algorithm to improve object tracking accuracy in video data [39–41]. It has been combined with the KF to provide better tracking continuity for beam aspect targets [42], or reduce the computational complexity of target positioning with multiple sensors [43]. A combined UKF-PF algorithm can be used to distinguish group targets using a surface radar [44].

Visual tracking is also a critical target-tracking task in computer vision applications, in which an object is usually tracked from images in real time. It also uses a tracker (e.g. the mean-shift procedure, KF, EKF, and PF) to track an object from images based on a target representation model. Different from typical target measurements by radar system, the target is usually represented by a feature space (e.g. color features, texture features or shape features) in the visual tracking area. The visual tracking could be quite challenging due to various factors, such as variance in the scene (e.g. illumination, occlusion, camouflage, background clutter), variance of target's appearance (e.g. scale, pose, deformation of non-rigid objects), bad image quality, online processing requirement, changing camera, and so on [45]. In order to provide robust long-term tracking under the situation with complicated change of target appearance and background, several state-of-the-art algorithms can be used, including the multiple instance learning (MIL) tracking, visual tracking decomposition (VTD), and ensemble tracking. The MIL tracking uses a positive bag consisting of several image patches to update a MIL classifier in applications such as face detection [46]. The VTD uses multiple observation models, multiple basic motion models and multiple basic trackers to deal with scenarios with severe pose variation, abrupt motions, occlusion, and illumination changes [47]. Ensemble tracking combines an ensemble of weak classifiers into a strong classifier to better distinguish the object

and background [48].

In 2000, an algorithm with a kernel-based histogram model and a Bhattacharyya coefficient based similarity function was proposed by Comaniciu [49] for real-time tracking of non-rigid objects using the mean shift method. In 2002, Perez [50] integrated this color-based model and the Bhattacharyya coefficient-based function into the probabilistic framework of PF to improve tracking robustness and versatility. In 2002, Nummiaro [51] improved this PF based visual tracking method using an adaptive reference target model. Since then, this PF based visual tracking algorithm that employs the color histogram based target model and Bhattacharyya coefficient based similarity distance has been much studied in the literature [52–58]. Although this PF-based visual tracking approach has been studied widely in different aspects for computer vision applications, it has not been used in target tracking from nautical radar images.

In this thesis, a PF based visual tracking method is sought to provide a reliable and effective target tracking from the nautical radar images. Different from the general visual tracking application, the change of the target appearance and the clutter (sea clutter) background is usually not that severe in nautical radar tracking. The size, shape or intensities of the radar target changes slowly through the radar image sequence. The target is usually quite small in terms of the number of pixels. Thus, a computationally efficient algorithm is preferred, satisfying the requirement of tracking accuracy and robustness in the meantime. Instead of using the above-mentioned sophisticated algorithms such as MIL and VTD, the proposed PF based visual tracking algorithm employs the kernel-based histogram model to represent a target in the radar images, and the Bhattacharyya coefficient based similarity function between reference and candidate target models to provide the likelihood function for the particle filtering.

1.3 Scope of Thesis

In this thesis, the scope of the study is limited to tracking a single maneuvering target from scan-converted X-band nautical radar images with limited scenarios and environments. This study focuses on the implementation of the basic tracking process with the particle filter based visual tracking strategy. In order to evaluate the performance of the proposed algorithms, a simple implementation of the classical tracking approach is also employed for comparison. Furthermore, the tracking results are also compared with GPS data.

In Chapter 2, a classical approach for target tracking from nautical radar images is presented. This tracking approach employs the order-statistics CFAR processing to detect target signals from the radar images, and the Kalman filter to estimate target position and velocity based on a constant-acceleration (CA) motion model in the linear Gaussian dynamic tracking system. In addition, an adaptive KF algorithm is integrated to deal with the maneuvering target motion.

In Chapter 3, a visual tracking strategy is integrated in a particle filter framework to design a particle filter-only based target tracking method from X-band nautical radar application. The tracking method employs a kernel-based histogram model to represent the target, and a Bhattacharyya coefficient based distance to provide the likelihood function for the particle filtering. Two algorithms are developed to implement the PF-only based tracking approach: one can only estimate target position [59, 60] and the other one can extract both position and velocity [61, 62].

In Chapter 4, a combined PF-KF approach is designed to estimate both target position and velocity [63]. With this approach, the dimension of state vector for PF sampling is reduced. In order to improve the tracking accuracy, stability, and flexibility, multiple methods such as enhanced target model construction, updating reference target model, and adaptive KF filtering for maneuvers, are also proposed.

In Chapter 5, the tracking performance of the above-mentioned KF-based classical tracking approach, the proposed PF-only and PF-KF based visual tracking approaches is analyzed using the scan converted nautical images collected by a land-based X-band nautical system. These tracking results are compared with shipborne GPS data during the experiments.

The overall conclusions from the research in this thesis are presented in Chapter 6, in which some suggestions for future work are also outlined.

Chapter 2

KF Based Classical Tracking Approach

In this chapter, the classical target tracking process used by a nautical radar is first introduced briefly. Next, the target detection techniques based on OS-CFAR and the Kalman filter tracking method are described. Finally, the detailed design of a KF based classical tracking approach for nautical radar application is presented.

2.1 Introduction

In nautical radar applications, target tracking can be performed after targets are detected from the radar data. This process can be demonstrated by three successive modules (signal processor, data extractor, and data processor) in the receiving phase of a modern monostatic radar system (see Fig. 2.1) [1]. In the signal processor module, the target and clutter signals are first discriminated by some basic operations (e.g. constant false alarm rate (CFAR)). Then the data extractor module provides the radar measurements (typically called "plot" for radar tracking applications), such as target

range, azimuth. With the obtained target measurements, the data processor module employs a tracking filter to provides refined target information (e.g., target position, speed and heading) on the radar display (e.g., plan position indicator (PPI), etc.).

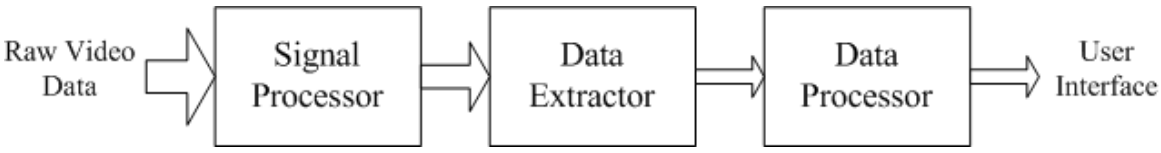

Figure 2.1: Data flow in the receiving phase of a monostatic radar system.

In the past, the target position was marked by the radar operator manually, which has obvious limitations in tracking accuracy and capacity. In modern radar tracking systems, the tracking process needs to be automatically performed based on several basic tracking steps, including track initialization, track smoothing (or track filtering), and track maintenance (or track termination) [64]. In the track initialization step, a track is established with the initial state of the target being determined. Then, the target's kinematic parameters are estimated, in the track smoothing step, by a tracking filter based on the track prediction with target motion model and updated measurements (plots). If the target is not seen in several consecutive scans, the track could be dropped in the track maintenance step. As an example, the track-while-scan (TWS) system, incorporating the above basic steps, is a typical tracking system in providing tracks of a single target or multiple targets while maintaining radar scanning simultaneously [65].

In this thesis, a relatively simple implementation of the above classical tracking strategy is designed to obtain position and velocity of a single target from scan-converted (Cartesian) X-band nautical radar images. It is used as a comparison method for the proposed PF based algorithms in the following chapters. For this simple implementation, only OS-CFAR processing in the signal processor module is

employed to process the radar images to obtain target signals. Then the centroid of the target signals is used to provide the specific target center coordinates in the data extractor module. In the data processor module, the Kalman filter is used to estimate the target position and velocity based on a constant-acceleration (CA) target motion model. Moreover, the approximate initial position of the target is assumed to be known, and the target is assumed to exist throughout the radar image sequences.

2.2 Target Detection

The constant false alarm rate (CFAR) detector is widely used to perform target detection in radar signal processing systems. Conventionally, the cell-average CFAR (CA-CFAR), as a one-parameter CFAR, is the simplest CFAR scheme. In the CA-CFAR, the average of the reference cells surrounding the cell under test (CUT) multiplied by a scale factor, the resultant value is compared with the pixel intensity of the CUT in the radar image. If the CUT has higher intensity than the threshold, it implies the presence of a target signal. For the CA-CFAR processing of a radar image, the reference cells are set as a moving squared window with the CUT in the center. Each pixel in the radar image would be treated as the CUT and processed by CFAR processing. However, the detection performance of this conventional CA-CFAR scheme would be degraded significantly when an interfering target or abrupt clutter change is present in the reference window. In order to deal with this problem, some other CFAR schemes have been proposed, including the greatest-of (GO) CFAR, smallest-of (SO) CFAR, ordered-statistics (OS) CFAR and the trimmed-mean (TM) CFAR. Among these CFAR schemes, the OS-CFAR is considered to perform best in dealing with interfering targets and the clutter change problem [13]. Thus, the OS-CFAR scheme is adopted in this thesis to represent target detection for the classical tracking

approach.

Firstly, the OS-CFAR sorts the reference elements surrounding the CUT in the window in an ascending or a descending order. Then, the kth element, instead of the average of reference cells in CA-CFAR scheme, is selected for the CFAR threshold determination. This scheme can effectively alleviate the impact of large target, multiple targets or abrupt clutter. In this research, the median element of the reference cells is selected.

The setting of the scale factor will affect the detection performance and the probability of false alarm. Basically, a large scale factor would decrease the probability of false alarm and probability of detection. On the contrary, a small scale factor would increase the probability of false alarm and probability of detection. In order to evaluate the performance of the CFAR schemes and determine appropriate thresholds, an experimental method is used to evaluate the performance of the CA-CFAR and OS-CFAR detectors with the probability of detection P_d against the probability of false alarm P_{fa}, by using varied scale factors (i.e. varied thresholds). As the detection problem could be treated as a binary statistical test problem with hypothesis H_0 (target is absent) and hypothesis H_1 (target is present), P_{fa} and P_d could be expressed as joint probability density functions

$$P_{fa} = P(X > X_T|H_0) \tag{2.1}$$

$$P_d = P(X > X_T|H_1) \tag{2.2}$$

where X denotes the intensity of a pixel in the radar image and X_T is the threshold. The probability of false alarm rate and the probability of detection can be evaluated

experimentally using

$$P_{fa} = \frac{\text{False Target Cells Detected}}{\text{Total Clutter Cells}} \tag{2.3}$$

$$P_d = \frac{\text{Correct Target Cells Detected}}{\text{Total Target Cells}} \tag{2.4}$$

After the target signals are detected in the radar images by CFAR processing, the target center position is calculated as a weighted centroid of detected target signals in a square region around the predicted position. The definition of the centroid is

$$x_k^m = \frac{\sum_{i=1}^{N} x_{k,t}^i h_{k,t}^i}{\sum_{i=1}^{N} h_{k,t}^i} \tag{2.5}$$

$$y_k^m = \frac{\sum_{i=1}^{N} y_{k,t}^i h_{k,t}^i}{\sum_{i=1}^{N} h_{k,t}^i} \tag{2.6}$$

where x_k^m and y_k^m are calculated target center coordinates along the x axis and y axis of the scan-converted radar image at time k, N denotes the number of detected target signals here, $x_{k,t}^i$ and $y_{k,t}^i$ denote the x and y coordinates of a detected "target" signal, respectively, $h_{k,t}^i$ denotes the intensity of the target pixel.

2.3 Kalman Filter

The tracking filter in the Data Processor module is a fundamental function in Radar Data Processing systems. It processes the target radar measurements (e.g. range, azimuth) to reduce the measurement errors, estimate the target velocity and predict future target position.

In order to help understand the concept of a tracking filter in radar applications, an α-β filter, as a preliminary algorithm for practical radar tracking applications, is introduced here. This filter is the simplest tracker, for which the target is assumed to move along a straight line (along the x axis for simplicity) with a constant speed. It can be described by [9]

$$x_k^s = x_k^p + \alpha(x_k^m - x_k^p) \tag{2.7}$$

$$\dot{x}_k^s = \dot{x}_{k-1}^s + \beta(x_k^m - x_k^p)/T \tag{2.8}$$

$$x_{k+1}^p = x_k^s + \dot{x}_k^s T \tag{2.9}$$

where x_k^s is the smoothed position, $\dot{x}_k^s$ is the smoothed velocity, x_k^p is the predicted position, x_k^m is the measured position, T is a fixed radar scanning period, and α and β are the system gains, which usually take value between [0, 1]. From the above equations, it can be found that filtering behavior depends on the determination of the α and β. In the extreme cases, the filtered position and velocity approach the measured position when both gains are set to 1, and approach the predicted results when they are set to 0. This α-β filter is limited to track a maneuvering target, but it can still be found in practical applications on account of its simplicity. The α-β filter does not require a system model and is a simplified Kalman filter [64].

In oder to introduce the Kalman filter, the general dynamic system for a tracking problem can be modeled as

$$\boldsymbol{s}_k = \boldsymbol{f}_k(\boldsymbol{s}_{k-1}, \boldsymbol{u}_{k-1}) \tag{2.10}$$

$$\boldsymbol{z}_k = \boldsymbol{h}_k(\boldsymbol{s}_k, \boldsymbol{v}_k) \tag{2.11}$$

where $\boldsymbol{f}_k(\cdot)$ and $\boldsymbol{h}_k(\cdot)$ denote the state transition function and measurement function, respectively, $\boldsymbol{s}_k$ is the state vector at time k ($k \in \mathbb{N}$), $\boldsymbol{z}_k$ is the updating observation, and $\boldsymbol{u}$ and $\boldsymbol{v}$ represent process noise and measurement noise with known distributions,

respectively [66].

If the state transition function $\boldsymbol{f}_k(\cdot)$ and the measurement function $\boldsymbol{h}_k(\cdot)$ are linear, and the process noise $\boldsymbol{u}$ and measurement noise $\boldsymbol{v}$ are mutually independent Gaussian noise with zero mean and known variances, this dynamic system is called a linear-Gaussian system. The optimal solution of this linear-Gaussian system based on the mean square error (MSE) estimation criteria is the Kalman filter, which can be given by [1]

$$\boldsymbol{s}_{k|k} = \boldsymbol{s}_{k|k-1} + \boldsymbol{K}_k(\boldsymbol{z}_k - \boldsymbol{H}_k\boldsymbol{s}_{k|k-1}) \tag{2.12}$$

$$\boldsymbol{P}_{k|k} = \boldsymbol{P}_{k|k-1} - \boldsymbol{K}_k\boldsymbol{H}_k\boldsymbol{P}_{k|k-1} \tag{2.13}$$

with

$$\boldsymbol{s}_{k|k-1} = \boldsymbol{F}_k\boldsymbol{s}_{k-1|k-1} \tag{2.14}$$

$$\boldsymbol{P}_{k|k-1} = \boldsymbol{Q}_{k-1} + \boldsymbol{F}_k\boldsymbol{P}_{k-1|k-1}\boldsymbol{F}_k^T \tag{2.15}$$

$$\boldsymbol{K}_k = \boldsymbol{P}_{k|k-1}\boldsymbol{H}_k^T(\boldsymbol{H}_k\boldsymbol{P}_{k|k-1}\boldsymbol{H}_k^T + \boldsymbol{R}_k)^{-1} \tag{2.16}$$

where $\boldsymbol{F}_k$ and $\boldsymbol{H}_k$ are the linear state transition function and measurement function, respectively. $\boldsymbol{P}_{k|k-1}$ and $\boldsymbol{P}_{k|k}$ are the covariance matrix of the estimation error before and after the measurement $\boldsymbol{z}_k$ is processed, $\boldsymbol{Q}$ and $\boldsymbol{R}$ are the covariances of the noise $\boldsymbol{u}$ and $\boldsymbol{v}$, respectively. $\boldsymbol{K}$ denotes the Kalman gain, which influences the filtering amplitude, and is determined by the ratio between the process noise and the measurement noise [1].

2.4 KF Based Tracking Algorithm

2.4.1 State space models

First, the system state and motion models are defined for the state transition function in Eq. (2.10). As the target position and velocity are required in the tracking system, the state vector for the tracking problem in scan-converted (Cartesian) radar images is defined as

$$\boldsymbol{s}_k = [x_k, \dot{x}_k, y_k, \dot{y}_k]^T \tag{2.17}$$

where x_k and y_k denote the target's center coordinates along the x- and y-axis in the radar image, and $\dot{x}_k$ and $\dot{y}_k$ denote the target's velocities along the x- and y-axis, respectively.

In order to model the maneuvering of a target here, a constant-acceleration motion model is employed as the state transition function [33],

$$\boldsymbol{s}_k = \begin{bmatrix} 1 & T & 0 & 0 \\ 0 & 1 & 0 & 0 \\ 0 & 0 & 1 & T \\ 0 & 0 & 0 & 1 \end{bmatrix} \boldsymbol{s}_{k-1} + \begin{bmatrix} T^2/2 & 0 \\ T & 0 \\ 0 & T^2/2 \\ 0 & T \end{bmatrix} \begin{bmatrix} a_{x,k} \\ a_{y,k} \end{bmatrix} \tag{2.18}$$

where T denotes the scan interval between successive observations, $a_{x,k}$ and $a_{y,k}$ denote the target acceleration along the x- and y-axis, which are treated as independent zero-mean Gaussian noise. The initial center coordinates of the target x_0 and y_0 can be determined manually or in an automatic initialization scheme, while the initial velocities $\dot{x}_0$ and $\dot{y}_0$ are set to zero. From the definition of the function in Eq. (2.18), it can be found that the state transition function is linear with Gaussian noise.

Next, the measurement function in Eq. (2.11) can be defined based on the obtained

target observation (x_k^m and y_k^m) from CFAR processing and measurement noise $\boldsymbol{v}_k$ with known distribution. Thus, the measurement function of the dynamic system is chosen as

$$\boldsymbol{z}_k = \boldsymbol{H}_k \boldsymbol{s}_k + \boldsymbol{v}_k \tag{2.19}$$

with $\boldsymbol{z}_k = [x_k^m, y_k^m]^T$ and

$$\boldsymbol{H}_k = \begin{bmatrix} 1 & 0 & 0 & 0 \\ 0 & 0 & 1 & 0 \end{bmatrix} \tag{2.20}$$

where $\boldsymbol{H}_k$ is the projection matrix from the current state to current measurement, which is linear. The observation noise $\boldsymbol{v}_k$ is also set as Gaussian-distributed with zero mean and variance σ_v^2, which is set to 4 empirically since too small or too large value would cause large error in the position and velocity estimation from our experiments.

Based on the above definitions of the state transition and measurement functions, it can be found that the dynamic system is linear and Gaussian. As a result, the Kalman filter would be a natural option as an optimal solution to this system.

2.4.2 Adaptive tracking for maneuvering target

In practical radar applications, the maneuvering of the target could be very uncertain as the acceleration of the target could vary significantly in an unpredictable way. In order to improve the tracking performance and stability, an adaptive algorithm is required to deal with the maneuvering target. This adaptive algorithm usually includes two basic steps: maneuver detection and a mean of achieving adaptivity when a maneuver is detected. Different methods can be used for both steps [67].

First, the target maneuver needs to be detected. A simple maneuver detection algorithm [1] is based on using an innovation term $\boldsymbol{\nu}_k$ at each iteration of the Kalman filter

$$\boldsymbol{\nu}_k = \boldsymbol{z}_k - \boldsymbol{H}_k \boldsymbol{s}_{k|k-1} \tag{2.21}$$

where the covariance $\boldsymbol{\Theta}_k$ of the innovation term is defined as

$$\boldsymbol{\Theta}_k = \boldsymbol{H}_k \boldsymbol{P}_{k|k-1} \boldsymbol{H}_k^T + \boldsymbol{R}_k \tag{2.22}$$

The innovation sequence $\boldsymbol{\nu}_k$ is assumed to have a Gaussian distribution with zero mean and covariance matrix $\boldsymbol{\Theta}_k$ for a straight-line constant-speed moving target. If any (e.g. i-th) component of the innovation matrix is out of its corresponding interval $[-C\sqrt{\boldsymbol{\Theta}_k(i,i)}, C\sqrt{\boldsymbol{\Theta}_k(i,i)}]$ (C is a positive constant, and it is set to 1 in our experiments), a maneuver is considered to be happening.

Another maneuver detector used in many adaptive tracking algorithms is based on the normalized square residual of the innovation sequence [68]

$$\delta_k \triangleq \boldsymbol{\nu}_k^T \boldsymbol{\Theta}_k \boldsymbol{\nu}_k \tag{2.23}$$

where, δ_k is the square residual of the innovation sequence. Since the innovation term is assumed as normally distributed, the δ_k will be chi-square distributed with m degree of freedom (m is the dimension of the measurement or $\boldsymbol{\nu}_k$).

With δ_k, the fading memory average over the sliding window $[k-\Delta+1, k]$ of the square residual sequnce can be obtained using

$$g_k = \rho_w g_{k-1} + \delta_k \tag{2.24}$$

where ρ_w is the coefficient to determine the effective length of the fading memory Δ ($\Delta = (1-\rho_w)^{-1}$).

If g_k is larger than a certain threshold, a maneuver is thought to exist sometime between the time $k-\Delta+1$ to current time k.

After the maneuver is detected, a variety of techniques can be used for the adaptive

filtering, including adaptive process noise [69], augmentation of the state vector [68], multiple filters, or the interacting multiple model (IMM) algorithm [70]. In this thesis, the adaptive process noise method is used. When a target maneuver is detected, the variance of the process noise $\boldsymbol{u}_k$ is increased to make the estimated result approach the measured observation more, instead of the past history, i.e. the predicted state, which is considered to be relatively less reliable in that case. If the process noise is not increased, the estimated results would be less accurate based on the MSE criteria.

Both the innovation term $\boldsymbol{\nu}_k$ based detection and the residual δ_k based detection methods have been tested for use in the KF-based classical tracking approach. Comparison of results from two maneuver detection methods shows similar tracking performance. Thus, only the innovation term-based maneuver detection method is adopted in this thesis for its smaller computational load.

2.4.3 Summarization of the algorithm

The proposed classical tracking approach based on the Kalman filter defined above can be implemented by the following iterative steps:

Determine the initial target center coordinates and velocities in the first radar image;

FOR k=2:ImageNumber

1. **Predict** next positions and velocities based on Eq. (2.18);
2. **Detect** the maneuver based on Eq. (2.21), and adjust the measurement function if maneuver is detected;
3. **Estimate** target center coordinates x_k, y_k and velocities $\dot{x}_k$, $\dot{y}_k$ based on obtained measurements in a new radar image using Eq. (2.19) and Eqs. (2.12)-(2.16);

END

The test results from this KF-based classical tracking approach using practical X-band nautical radar image sequences will be illustrated in Chapter 5, in which the tracking results will also be compared with those of the proposed PF-based visual tracking approaches and GPS data.

Chapter 3

PF-only Based Visual Tracking Approaches

In this chapter, a particle filter only based visual tracking approach is proposed to estimate target position and velocity from nautical radar images. The formulations of the SIR particle filter are first introduced briefly. Then, a PF-only based tracking approach is designed for estimation of target position only, using an auto-regressive motion model [59, 60]. Furthermore, an improved PF-only based visual tracking approach is developed to estimate both target position and velocity using a constant-acceleration motion model [61, 62].

3.1 SIR Particle Filter

The particle filter, employing the sequential importance sampling technique to approximate relevant probability distributions with a set of random samples, is particularly useful to deal with a recursive Bayesian state estimation (filtering) problem for a non-linear non-Gaussian dynamic system [32]. As shown in Chapter 2, the evolution of

the dynamic system states can be defined as

$$\boldsymbol{s}_k = \boldsymbol{f}_k(\boldsymbol{s}_{k-1}, \boldsymbol{u}_{k-1}) \tag{3.1}$$

where $\boldsymbol{f}_k(\cdot)$ denotes a system state transition function, $\boldsymbol{s}_k$ denotes a state vector at current time step k ($k \in \mathbb{N}$), $\boldsymbol{u}_{k-1}$ denotes process noise vector with known Gaussian or non-Gaussian distribution. The measurement function is defined as

$$\boldsymbol{z}_k = \boldsymbol{h}_k(\boldsymbol{s}_k, \boldsymbol{v}_k) \tag{3.2}$$

where $\boldsymbol{h}_k(\cdot)$ denotes a linear or nonlinear measurement function, $\boldsymbol{z}_k$ denotes the observation measurements up to current time k, $\boldsymbol{v}_k$ is the measurement noise vector with known distribution [66]. For a radar target tracking problem, the state vector typically denotes kinematic information of the target, such as target position, velocity and acceleration, while the measurements are typically range, bearing, elevation or bearing rate (Doppler measurement) [25]. It is assumed that the current state for the system dynamics is only related to the previous state, and not future or other past states. Meanwhile, the measurement up to current time is only a function of the state up to the current time.

The filtering problem is equivalent to estimating the conditional posterior probability density function (PDF) $p(\boldsymbol{s}_k|\boldsymbol{z}_{0:k})$ based on a sequence of consecutive updating observations $\boldsymbol{z}_{0:k}$ and the system state-space models with state transition and measurement functions, assuming that the initial PDF $p(\boldsymbol{s}_0|\boldsymbol{z}_0) = p(\boldsymbol{s}_0)$ is available. The recursive Bayesian state estimation method for this filtering problem generally consists of two steps: prediction and updating.

The prediction step involves obtaining the predicted state density $p(\boldsymbol{s}_k|\boldsymbol{z}_{0:k-1})$ using the available posterior density $p(\boldsymbol{s}_{k-1}|\boldsymbol{z}_{0:k-1})$ at time $k-1$ and the state transition

function through the Chapman-Kolmogorov equation [31]

$$p(\boldsymbol{s}_k|\boldsymbol{z}_{0:k-1}) = \int p(\boldsymbol{s}_k|\boldsymbol{s}_{k-1})p(\boldsymbol{s}_{k-1}|\boldsymbol{z}_{0:k-1})d\boldsymbol{s}_{k-1} \tag{3.3}$$

For the updating step, the required density $p(\boldsymbol{s}_k|\boldsymbol{z}_{0:k})$ conditional on measurement up to time k is obtained via Bayes rule

$$p(\boldsymbol{s}_k|\boldsymbol{z}_{0:k}) = \frac{p(\boldsymbol{z}_k|\boldsymbol{s}_k)p(\boldsymbol{s}_k|\boldsymbol{z}_{0:k-1})}{p(\boldsymbol{z}_k|\boldsymbol{z}_{0:k-1})} \tag{3.4}$$

With the obtained posterior density $p(\boldsymbol{s}_k|\boldsymbol{z}_{0:k})$, the moments of the state vector could be estimated. For example, the mean of the states is calculated by

$$\hat{\boldsymbol{s}}_k = E(\boldsymbol{s}_k|\boldsymbol{z}_{0:k}) = \int \boldsymbol{s}_k p(\boldsymbol{s}_k|\boldsymbol{z}_{0:k})d\boldsymbol{s}_k \tag{3.5}$$

The Kalman filter is the optimal solution for the filtering problem assuming the state transition function and measurement function are linear and the process noise and measurement noise are additively Gaussian distributed with zero mean and known covariances [31]. In real-world situations, this assumption is rarely valid. As a result, improved Kalman filters with some approximation techniques, such as the extended Kalman filter (EKF) and unscented Kalman filter (UKF) algorithm, could be employed as suboptimal solutions. However, these Kalman filter-based methods could not adequately approximate relevant probability distributions when the linearity of the functions are weak or the noise distributions are greatly different from the Gaussian distribution.

The particle filter, as a sequential Monte Carlo method, can effectively approximate the desired probability distributions using the importance sampling principle. It describes the posterior density $p(\boldsymbol{s}_k|\boldsymbol{z}_{0:k})$ with discrete weighted samples $\{\boldsymbol{s}_k^i, w_k^i\}_{i=1}^{N_s}$

$$p(\boldsymbol{s}_k|\boldsymbol{z}_{0:k}) \approx \sum_{i=1}^{N_s} w_k^i \delta(\boldsymbol{s}_k - \boldsymbol{s}_k^i) \tag{3.6}$$

where $\boldsymbol{s}_k^i$ denotes a sample with an associated weight w_k^i, and N_s is the number of samples. Note that the weights of the samples should be normalized to ensure $\sum_{i=1}^{N_s} w_k^i = 1$. Asymptotically, these random samples with associated weights of particle filter could approach the true probability density if the sample number approaches infinity.

As the posterior density is difficult to draw samples from, the importance sampling principle of the Monte Carlo approach is employed with an importance density $q(\boldsymbol{s}_{0:k-1}|\boldsymbol{z}_{0:k-1})$ for the density $p(\boldsymbol{s}_{0:k-1}|\boldsymbol{z}_{0:k-1})$ at time $k-1$. Then, the weights update at time k for the filtering problem would be derived as [31]

$$w_k^i \propto w_{k-1}^i \frac{p(\boldsymbol{z}_k|\boldsymbol{s}_k^i)p(\boldsymbol{s}_k^i|\boldsymbol{s}_{k-1}^i)}{q(\boldsymbol{s}_k^i|\boldsymbol{s}_{k-1}^i, \boldsymbol{z}_k)} \tag{3.7}$$

Consequently, the sequential importance sampling (SIS) algorithm of the particle filter could be described with two steps: firstly drawing samples $\boldsymbol{s}_k^i$ from the importance density $q(\boldsymbol{s}_k|\boldsymbol{s}_{k-1}^i, \boldsymbol{z}_k)$, and secondly updating weights w_k^i according to Eq. (3.7).

In this thesis, the sampling importance resampling (SIR) particle filter is applied, choosing the prior $p(\boldsymbol{s}_k^i|\boldsymbol{s}_{k-1}^i)$ as the importance density $q(\boldsymbol{s}_k^i|\boldsymbol{s}_{k-1}^i, \boldsymbol{z}_k)$, which is one of the most frequently used densities [66]. Accordingly, the weights are updated from Eq. (3.7) as

$$w_k^i \propto w_{k-1}^i p(\boldsymbol{z}_k|\boldsymbol{s}_k^i) \tag{3.8}$$

Furthermore, the systematic resampling method [31] for each iteration is adopted for the SIR filter to mitigate the particle degeneracy problem, where a large portion of particles are associated with negligible weights.

3.2 Target Position Estimation

3.2.1 State transition model

The state transition function defines the evolution of system states. For a typical target-tracking application, a constant-velocity (CV) model is commonly used with the system state vector of interest denoting the motion characteristics of the moving target, including target position and velocity [33]. In this approach, only the target center position is estimated. Thus the state vector in Eq. (3.1) is defined as

$$\boldsymbol{s}_k = [x_k, y_k]^T \tag{3.9}$$

where $[x_k, y_k]^T$ denotes the target center position's x and y coordinates in the Cartesian radar image at time k, respectively.

Since the main purpose here is to estimate the target positions, an auto-regressive state transition function [50, 58] is used for Eq. (3.1)

$$\boldsymbol{s}_k = \boldsymbol{s}_{k-1} + \Delta\boldsymbol{s}_{k-1} + \boldsymbol{u}_{k-1} \tag{3.10}$$

where $\Delta\boldsymbol{s}_{k-1} = \boldsymbol{s}_{k-1} - \boldsymbol{s}_{k-2}$ denotes the moving distance of the last two states with initial $\Delta\boldsymbol{s}_0 = (0, 0)^T$, $\boldsymbol{u}_{k-1}$ denotes the zero-mean Gaussian white-noise sequence with a predefined covariance $\boldsymbol{Q}_{k-1} = \sigma_u^2\boldsymbol{I}$ [66]. The $\boldsymbol{I}$ is a 2×2 identity matrix, while the process noise standard deviation σ_u is set to 10 from the moving velocity of the target empirically since too large or small value would cause large error in the position estimation from our experiments.

3.2.2 Measurement model

Unlike the classical target tracking problem, the measurement model employs comparison between the reference target model and the target candidate as the state

measurement for this nautical radar visual tracking task. The target can be represented by a normalized B-bin histogram $\hat{\boldsymbol{q}} = [\hat{q}_1, \hat{q}_2, ..., \hat{q}_B]$ (u is the index of the histogram) of a square region around the target in the radar image with $\sum_{u=1}^{B} \hat{q}_u = 1$. The bin number B is related to the feature of the target and set to 16 in this paper empirically since useful target feature information could be lost if the bin number is too small or too large. This number can be different for a different target in different radar data.

The Bhattacharyya coefficient based histogram similarity distance $D(\hat{\boldsymbol{p}}, \hat{\boldsymbol{q}})$, measuring the difference of the reference target model and target candidate, can be defined as [71]

$$D(\hat{\boldsymbol{p}}, \hat{\boldsymbol{q}}) = \sqrt{1 - \rho[\hat{\boldsymbol{p}}, \hat{\boldsymbol{q}}]} \tag{3.11}$$

where $\hat{\boldsymbol{p}}$, $\hat{\boldsymbol{q}}$ are normalized histogram models of the candidate and reference target region, respectively, and $\rho[\hat{\boldsymbol{p}}, \hat{\boldsymbol{q}}]$ denotes the Bhattacharyya coefficient with

$$\rho[\hat{\boldsymbol{p}}, \hat{\boldsymbol{q}}] = \sum_{u=1}^{B} \sqrt{\hat{p}_u \hat{q}_u} \tag{3.12}$$

The Bhattacharyya coefficient can be interpreted as the cosine of the angle between $\sqrt{\hat{\boldsymbol{q}}}$ and $\sqrt{\hat{\boldsymbol{p}}}$ [72]. This Bhattacharyya coefficient based similarity distance can be used as a metric, as it is symmetric, simple to compute, bounded between $[0, 1]$, avoids singularity when a empty histogram exits, and obeys the triangle inequality [71].

Based on the defined similarity distance between the reference target model and each target candidate, the likelihood probability $p(\boldsymbol{z}_k|\boldsymbol{s}_k^i)$ of the measurement function of the particle filter is then defined as

$$p(\boldsymbol{z}_k|\boldsymbol{s}_k^i) = \frac{1}{\sigma_m \sqrt{2\pi}} e^{-D^2/(2\sigma_m^2)} \tag{3.13}$$

where D is the above-defined similarity distance. The variance of the white noise of the measurement function σ_m^2 is set to 1/60 to provide sufficient discrimination.

In order to construct the target model for the particle filter, the kernel-based histogram and background-weighted histogram distribution models are used.

3.2.3 Kernel-based histogram target model

The procedure is as follows: The kernel-based histogram scheme in [71] is first used to model the target. Assuming that pixel intensities far from the center position are less reliable, the target window of interest is masked with an isotropic kernel function in order to integrate the position information in the histogram of the target model. This kernel-based histogram is defined as [71]

$$\hat{q}_u = C \sum_{i=1}^{M} k\left(\left\|\frac{\boldsymbol{l} - \boldsymbol{l}_i}{h}\right\|^2\right) \delta(b(\boldsymbol{l}_i) - u) \tag{3.14}$$

where $k(\cdot)$ denotes a kernel function (a Gaussian kernel function is selected in this paper), $\boldsymbol{l}$ denotes the center of the target $(x, y)^T$, $\boldsymbol{l}_i$ denotes the position of a pixel within the square target window of interest, M denotes the total pixel numbers of the square or rectangle region surrounding the target, h denotes the bandwidth of the kernel function, involving the scale of the target window, $\delta(\cdot)$ is the Kronecker delta function, $b(\boldsymbol{l}_i)$ denotes the assignment of a pixel in the target window to corresponding bin index, and C denotes the normalization constant. In this approach, a square region with width W, instead of the elliptical region in [71], is used to formulate the histogram as the target appearance could change in different radar images. Thus, the kernel bandwidth h is set as $h = \sqrt{2}W/2$ to provide the range [0,1] for the kernel function. An example of the kernel-based reference target model construction is illustrated in Fig. 3.1.

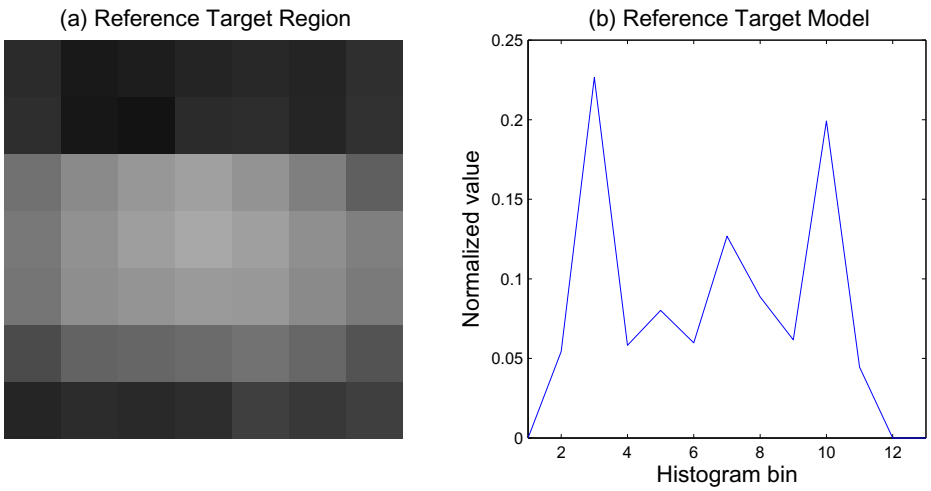

Figure 3.1: Kernel-based reference target model construction: (a)A reference target region; (b)Constructed normalized reference target model.

3.2.4 Background-weighted histogram target model

As the kernel-based histogram model integrates the geometry information in the target model, the determination of the center position and size of the reference target region is critical for the accuracy and stability of the tracking algorithm. In order to alleviate this dependence and improve the flexibility of the tracking algorithm, a background-weighted histogram model can also be proposed for the target representation. The model removes the bins of the original histogram that are lower than a threshold, which represents the information of clutter background surrounding the target. Equivalently, only pixels that have a larger intensity than the threshold are used to construct the target histogram model. As the background in nautical radar images is simple sea clutter, the threshold is indicated by the median intensity of the pixels within a square window surrounding the target. This pre-processing method for target model is similar to the OS-CFAR processing for target detection, as the median value is a good indicator of the background information compared with the mean value in the CA-CFAR. Then, the same similarity distance $D(\hat{\boldsymbol{p}}, \hat{\boldsymbol{q}})$ is used to form the likelihood probability of the measurement function for the particle filter.

By comparing the kernel-based model and the background-weighted model in [60], it is found that the kernel-based target model can help locate the center position of the radar target with a better tracking accuracy in target position estimation when the initial reference target model is determined accurately. However, the background-weighted histogram target model is more stable even when the reference target region is set inaccurately with inaccurate target center position or excessively large size. Thus, the kernel-based reference target model is adopted for the proposed visual tracking algorithms in this thesis.

3.2.5 Summarization of the algorithm

Based on the above-mentioned state transition function and measurement function, the SIR particle filter method is implemented to recursively estimate the target position, with the following steps for each estimation iteration:

Determine the initial target center coordinates and the reference target model from the reference target region in the first radar image, manually;

FOR k=2:ImageNumber

1. **Predict** next positions with the sampling of the prior density $p(\boldsymbol{s}_k^i|\boldsymbol{s}_{k-1}^i)$ based on Eq. (3.10);
2. **Update** particle weights using Eq. (3.8) based on the likelihood function Eq. (3.13) and normalize the weights;
3. **Resample** weights with the systematic method [31];
4. **Estimate** the target center coordinates from the weighted samples $\{\boldsymbol{s}_k^i, w_k^i\}_{i=1}^{N_s}$;

END

3.3 Target Position and Velocity Estimation

The previously proposed approach can only estimate the target position. However, the velocity information of the target is usually required in practical nautical radar applications. As a result, the PF-only based visual tracking approach is further modified for estimating both target position and velocity [61, 62].

3.3.1 State transition model

The second-order autoregressive function in [60] is not used anymore since target velocity also needs to be estimated, and it should be included in the state vector. Thus, the state vector in Eq. (3.1) is defined as

$$\boldsymbol{s}_k = [x_k, \dot{x}_k, y_k, \dot{y}_k]^T \tag{3.15}$$

Then, a constant-acceleration model is employed as the state transition function to describe the maneuvering motion of the target [33].

$$\boldsymbol{s}_k = \begin{bmatrix} 1 & T & 0 & 0 \\ 0 & 1 & 0 & 0 \\ 0 & 0 & 1 & T \\ 0 & 0 & 0 & 1 \end{bmatrix} \boldsymbol{s}_{k-1} + \begin{bmatrix} T^2/2 & 0 \\ T & 0 \\ 0 & T^2/2 \\ 0 & T \end{bmatrix} \begin{bmatrix} a_{x,k} \\ a_{y,k} \end{bmatrix} \tag{3.16}$$

where $a_{x,k}$ and $a_{y,k}$ denote the target acceleration along the x- and y-axis, which are treated as independent zero-mean Gaussian noise. The initial center coordinates of the target x_0 and y_0 are determined automatically with the initial velocities $\dot{x}_0$ and $\dot{y}_0$ set to zero.

3.3.2 Measurement model

As in Section 3.2.2, the observation model of this approach also employs the kernel-based histogram models for the reference and candidate targets using Eq. (3.14). Thus, the same likelihood function $p(\boldsymbol{z}_k|\boldsymbol{s}_k^i)$ (i.e. Eq. (3.13)) from the Bhattacharyya coefficient based histogram similarity distance $D(\hat{\boldsymbol{p}}, \hat{\boldsymbol{q}})$ (Eq. (3.11)) between the reference and candidate target models is also used.

3.3.3 Improved reference target model

In [60], it is suggested that the target geometry be integrated into the histogram model since the tracking performance significantly depends on the accuracy of the reference target model. In [60], the reference target model was determined manually by setting a rectangular target region to closely cover the target. In order to increase the flexibility of the tracking algorithm, an automatic initialization scheme of the reference model is implemented based on a CFAR operation. Assuming a target exists in the initial radar image, CFAR processing is used to determine the target signals within a coarse target region surrounding the target. Then the centroid of target signals is used as the initial center position, and the width of the square reference target region is determined by calculating the amount of the target signals. With the initial center position and the size of the target region determined, the reference target model can be constructed using Eq. (3.14). Furthermore, an enhanced reference target model is proposed to exclude the influence of the clutter signals that fall in the determined reference target region. Due to unknown shape of the target, the size of the reference region, which is determined in the automatic scheme, needs to be set large enough to cover the reference target. Thus, unwanted clutter may still be included in the reference target region. The enhanced reference target model is constructed by only the target signals,

which are determined by CFAR processing. In Fig. 3.2, an example of the enhanced reference target model is shown. The reference target region used is the same as that in Fig. 3.1, but some clutter signals have been removed using CFAR processing.

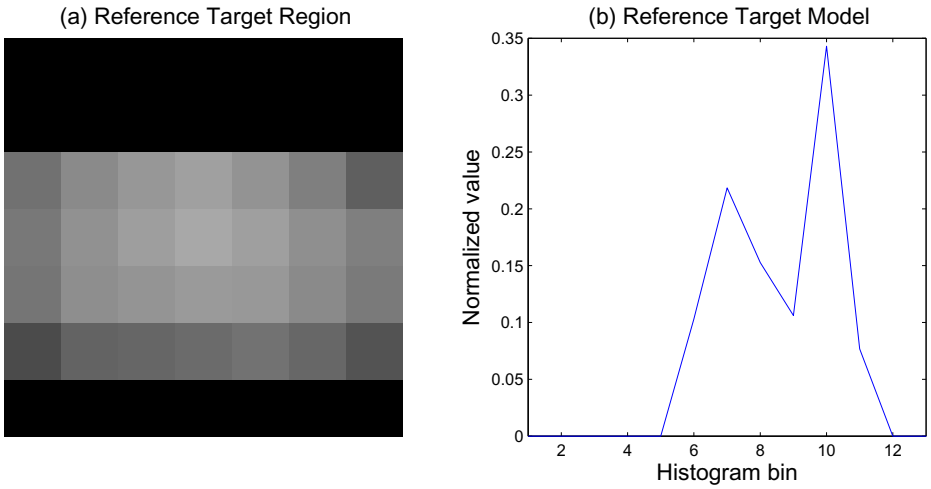

Figure 3.2: Enhanced kernel-based reference target model construction: (a)Reference target region without clutter signals; (b)Enhanced reference target model.

Within an image sequence, the appearance of the target may change gradually due to the change of the distance between the target and radar. In order to deal with this target's appearance change, the reference target model $\hat{\boldsymbol{q}}_k$ is updated using [34]

$$\hat{\boldsymbol{q}}_k = \hat{\boldsymbol{q}}_{k-1}(1-\alpha_r) + \hat{\boldsymbol{p}}_k\alpha_r \tag{3.17}$$

where $\hat{\boldsymbol{p}}_k$ is the current target model based on current estimation, and α_r is an adaptive coefficient, which is between 0 and 1. This adaptive coefficient needs to be set small (e.g. 0.1) since large α_r (e.g. 0.5) may cause divergence in target tracking (drift problem) due to the accumulation of inaccurate estimation of new target models $\hat{\boldsymbol{p}}_k$, especially for nautical radar applications with unknown background sea clutter.

3.3.4 Summarization of the algorithm

With the above-mentioned modification, the complete implementation procedure of this PF-only based procedure for position and velocity estimation approach can be summarized as

Determine the initial target center coordinates and velocities, and the kernel-based reference target model from the reference target region in the first radar image;
FOR k=2:ImageNumber

1. **Predict** next positions and velocities with the sampling of the prior density $p(\boldsymbol{s}_k|\boldsymbol{s}_{k-1}^i)$ based on Eq. (3.16);
2. **Update** particle weights using Eq. (3.8) based on the likelihood function Eq. (3.13) and normalize the weights;
3. **Resample** weights with the systematic method;
4. **Estimate** the target center coordinates x_k, y_k and velocities $\dot{x}_k$, $\dot{y}_k$ from the weighted samples $\{\boldsymbol{s}_k^i, w_k^i\}_{i=1}^{N_s}$;

END

In Chapter 5, this approach will also be tested based on field nautical radar image sequences and compared with other tracking algorithms.

Chapter 4

Combined PF-KF Based Visual Tracking Approach

As the PF method usually needs large computational cost, closely related to the number of the samples for particle filtering, a combined PF-KF method is proposed to reduce the computational cost and the risk of divergence by reducing the dimension of the state vector for particle filtering [63]. In this chapter, the detailed design of the combined PF-KF filter for the target position and velocity estimation is first presented. Then, modifications such as the enhanced reference target model construction and updating, and the adaptive KF method for dealing with maneuvers, are integrated to improve the tracking flexibility, robustness, and accuracy of the algorithm.

4.1 Target Tracking Problem Formulation

As in Chapter 3, the dynamic system for a tracking problem can generally be modeled as

$$\boldsymbol{s}_k = \boldsymbol{f}_k(\boldsymbol{s}_{k-1}, \boldsymbol{u}_{k-1}) \tag{4.1}$$

$$\boldsymbol{z}_k = \boldsymbol{h}_k(\boldsymbol{s}_k, \boldsymbol{v}_k) \tag{4.2}$$

Target tracking is to estimate the time-varying state vector $\boldsymbol{s}_k$ for the above dynamic system. It can be equivalent to estimating the conditional posterior probability density function (PDF) $p(\boldsymbol{s}_k|\boldsymbol{z}_{0:k})$ on sequential observations $\boldsymbol{z}_{0:k}$, assuming that the initial PDF $p(\boldsymbol{s}_0|\boldsymbol{z}_0) = p(\boldsymbol{s}_0)$ is available. This recursive Bayesian state estimation process generally consists of two steps: prediction and updating [31]. The prediction step obtains the predicted state density $p(\boldsymbol{s}_k|\boldsymbol{z}_{0:k-1})$ using the previous posterior density $p(\boldsymbol{s}_{k-1}|\boldsymbol{z}_{0:k-1})$ at time $k-1$ based on the state transition function. Then the updating step obtains the required density $p(\boldsymbol{s}_k|\boldsymbol{z}_{0:k})$ conditional on measurement up to time k via the Bayes rule

$$p(\boldsymbol{s}_k|\boldsymbol{z}_{0:k}) = \frac{p(\boldsymbol{z}_k|\boldsymbol{s}_k)p(\boldsymbol{s}_k|\boldsymbol{z}_{0:k-1})}{p(\boldsymbol{z}_k|\boldsymbol{z}_{0:k-1})} \tag{4.3}$$

4.2 State Transition Model

For nautical radar target tracking, which requires estimation of the target position and velocity from the Cartesian (scan-converted) radar image sequence, the state vector of the dynamic system in Eq. (4.1) is also chosen as

$$\boldsymbol{s}_k = [x_k, y_k, \dot{x}_k, \dot{y}_k]^T \tag{4.4}$$

where x_k, y_k denote the target center position's x and y coordinates in the Cartesian radar image at time k; $\dot{x}_k, \dot{y}_k$ denote the target velocity along the x axis and y axis, respectively. For our combined PF-KF tracking method, the target coordinates $[x_k, y_k]^T$ in the defined state vector are first estimated by the PF (in the following text $\boldsymbol{s}_k^{\mathrm{PF}} = [x_k, y_k]^T$).

In this approach, the state transition function also employs the constant-acceleration

(CA) model to describe the motion of the maneuvering target [33]

$$\boldsymbol{s}_k = \begin{bmatrix} 1 & 0 & T & 0 \\ 0 & 1 & 0 & T \\ 0 & 0 & 1 & 0 \\ 0 & 0 & 0 & 1 \end{bmatrix} \boldsymbol{s}_{k-1} + \begin{bmatrix} T^2/2 & 0 \\ 0 & T^2/2 \\ T & 0 \\ 0 & T \end{bmatrix} \begin{bmatrix} a_{x,k} \\ a_{y,k} \end{bmatrix} \tag{4.5}$$

where $a_{x,k}$ and $a_{y,k}$ denote the target acceleration along the x axis and y axis, which would be treated as independent zero-mean Gaussian noise to represent the uncertain movement of the target. Within the state transition function, the velocities can be obtained from the KF estimation after the PF estimation of target position in the combined PF-KF method.

4.3 PF Measurement Models

As in Chapter 3, the Bhattacharyya coefficient based histogram similarity distance $D(\hat{\boldsymbol{p}}, \hat{\boldsymbol{q}})$ between the reference target model $\hat{\boldsymbol{q}}$ and the candidate target model $\hat{\boldsymbol{p}}$ is also used for the measurement model in Eq. (4.2).

The candidate and reference target histogram model $\hat{\boldsymbol{p}}$ and $\hat{\boldsymbol{q}}$ are constructed using the kernel-based function in Eq. (3.14). Since this kernel-based model integrates the geometry in the target histogram model, the determination of the center position and size of the reference target region is critical for the accuracy and stability of the tracking algorithm. The automatic determination of the reference target region based on the CFAR processing in Chapter 3 is also implemented here. Then, the enhanced reference target model is constructed using Eq. (3.14) based on the determined reference target region with clutter signals removed.

Although the proposed histogram target model is relatively robust to the change

of target's pose and scale [52], and this target's appearance change through the radar image seuquence is usually not that severe as the general visual tracking application [45], the appearance of the target can still change gradually due to the change of the distance between the target and radar. Thus, the reference target model update method based on Eq. (3.17) is also used to deal with the target's change in appearance.

4.4 PF and KF Combining Procedure

As the measurement function described above is nonlinear, the particle filter method is employed to solve this non-linear system. The particle filter can approach the optimal Bayesian solution by approximating the posterior density $p(\boldsymbol{s}_k|\boldsymbol{z}_{0:k})$ in Eq. (4.3) with a set of discrete weighted samples $\{\boldsymbol{s}_k^{\mathrm{PF},i}, w_k^i\}_{i=1}^{N_s}$. Thus,

$$p(\boldsymbol{s}_k^{\mathrm{PF}}|\boldsymbol{z}_{0:k}^{\mathrm{PF}}) \approx \sum_{i=1}^{N_s} w_k^i \delta(\boldsymbol{s}_k^{\mathrm{PF}} - \boldsymbol{s}_k^{\mathrm{PF},i}) \tag{4.6}$$

where $\boldsymbol{s}_k^{\mathrm{PF},i}$ denotes a PF sample with an associated weight w_k^i and is a random position here, and N_s is the number of samples. Asymptotically, these weighted random samples (particles) can approach the true probability density when N_s approaches infinity.

Assuming the samples for the posterior density at time $k-1$ are available, the weight update for time step k at each iteration can be obtained with [31]

$$w_k^i \propto w_{k-1}^i \frac{p(\boldsymbol{z}_k^{\mathrm{PF}}|\boldsymbol{s}_k^{\mathrm{PF},i}) p(\boldsymbol{s}_k^{\mathrm{PF},i}|\boldsymbol{s}_{k-1}^{\mathrm{PF},i})}{q(\boldsymbol{s}_k^{\mathrm{PF},i}|\boldsymbol{s}_{k-1}^{\mathrm{PF},i}, \boldsymbol{z}_k^{\mathrm{PF}})} \tag{4.7}$$

where, $q(.)$ is the importance density.

In this approach, the standard SIR particle filter is applied for our application. It chooses the prior $p(\boldsymbol{s}_k^{\mathrm{PF},i}|\boldsymbol{s}_{k-1}^{\mathrm{PF},i})$ as the importance density $q(\boldsymbol{s}_k^{\mathrm{PF},i}|\boldsymbol{s}_{k-1}^{\mathrm{PF},i}, \boldsymbol{z}_k^{\mathrm{PF}})$, which is

one of the most frequently used densities [66]. Then the weights are updated with

$$w_k^i \propto w_{k-1}^i p(\boldsymbol{z}_k^{\mathrm{PF}} | \boldsymbol{s}_k^{\mathrm{PF},i}) \tag{4.8}$$

Furthermore, the SIR particle filter resamples the particles at each iteration to mitigate the particle degeneracy problem, where a large portion of particles are associated with negligible weights after the weight update.

Compared with other tracking filters for nonlinear system, such as EKF and UKF, the particle filter usually requires high computational cost, which is related to the dimension of the state vector for sampling. More particles are required when a state vector of higher dimension is used [33]. In order to reduce the computational cost and the risk of divergence, only the target position $[x_k, y_k]^T$ of the state vector $\boldsymbol{s}_k$ in Eq. (4.4) is sampled and estimated by the particle filter. After the preliminary target position is obtained, the Kalman filter can be used to further estimate the full state vector at each iteration.

In the proposed PF-KF procedure, the preliminary PF-estimated target coordinates $x_{k,z}$ and $y_{k,z}$ at each iteration can serve as the new observation $\boldsymbol{z}_k^{\mathrm{KF}} = [x_{k,z}, y_{k,z}]^T$ for the dynamic models of the Kalman filter to further estimate the target velocities in the state vector and refine the target positions. For the Kalman filter, the same state vector (Eq. (4.4)) and state transition function (Eq. (4.5)) are used but with a different measurement function

$$\boldsymbol{z}_k^{\mathrm{KF}} = \boldsymbol{H}_k \boldsymbol{s}_k + \boldsymbol{v}_k \tag{4.9}$$

in which

$$\boldsymbol{H}_k = \begin{bmatrix} 1 & 0 & 0 & 0 \\ 0 & 1 & 0 & 0 \end{bmatrix} \tag{4.10}$$

where $\boldsymbol{H}_k$ is the projection matrix from the current state to current measurement. The observation noise $\boldsymbol{v}_k$ is also set as Gaussian-distributed with zero mean and variance σ_v^2, which is set to 4 in our experiment. With the the linear-Gaussian system defined above, the analytic formulation of the Kalman filter to obtain the state vector can be found in Chapter 2.

4.5 Adaption for Maneuvering

In order to deal with the uncertain motion of the maneuvering target, the same adaptive filtering algorithm as in the classical KF-based approach (see Chapter 2) is employed in the KF estimation used in the combined PF-KF procedure. This algorithm employs the KF innovation term-based maneuver detection method and adaptive process noise to achieve adaptivity. For the maneuver detection method, it assumes the innovation sequence $\boldsymbol{\nu}_k$ of the Kalman filter has a Gaussian distribution with zero mean and covariance matrix $\boldsymbol{\Theta}_k$ for a straight-line constant-speed moving target. If any component of the innovation term is outside of its corresponding interval $([-C\sqrt{\boldsymbol{\Theta}_k(i,i)}, C\sqrt{\boldsymbol{\Theta}_k(i,i)}])$, a maneuver is considered to be happening. After the maneuver is detected, the variance of the process noise $\boldsymbol{u}_k$ is increased to put more weight on the measured observation, instead of the past history, i.e. the predicted state.

4.6 Implementation of the Combined PF-KF Algorithm

With scheme presented above, the combined PF-KF procedure for estimating target position and velocity can be implemented through the following iterative steps:

1. Determine the initial target center coordinates, velocity and the modified reference target model from the automatically determined reference target region;

2. Predict next positions by sampling the prior density $p(\boldsymbol{s}_k^{\mathrm{PF}}|\boldsymbol{s}_{k-1}^{\mathrm{PF},i})$ from the process noise in Eq. (4.5) and the initial velocity (set as zero here) for the first iteration or the velocities obtained by KF in step (6) for other iterations;

3. Update particle weights using Eq. (4.8) and normalize the weights;

4. Resample weights with the systematic method;

5. Calculate preliminary target coordinates from the weighted samples $\{\boldsymbol{s}_k^{\mathrm{PF},i}, w_k^i\}_{i=1}^{N_s}$;

6. Estimate the new target coordinates x_k, y_k and velocities $\dot{x}_k$, $\dot{y}_k$ using the KF;

7. Return to step 2 and update time $k = k + 1$.

The results of this PF-KF based visual tracking approach using field nautical radar images will be presented and discussed in Chapter 5, in which comparison with the PF-only based visual tracking approach, the classical KF based tracking approach and GPS data will also be provided.

Chapter 5

Experimental Results and Discussion

In this chapter, the tracking results of the classical KF based approach, the proposed PF-only and PF-KF based visual approach using field nautical radar data are illustrated and compared with GPS data. First, the field nautical radar images and the GPS data for testing are described. Then, the tracking performance of these three algorithms is evaluated and discussed.

5.1 Experiment Data

5.1.1 Radar image sequences

In order to evaluate the performance of the proposed PF-KF and PF-only based visual tracking approaches for nautical radar application, seven sequences of scan-converted radar images, which were collected by a land-based X-band nautical radar system on the Canadian East Coast in March, 2010, are tested. These data were collected under varying sea clutter levels, different range resolutions and antenna rotation periods

with varying target distances (see Table 5.1). The data, in which the target (a ship) is moving with a piecewise constant radius and speed around the radar, is denoted as "CRT", while the data with the ship moving with an abrupt turning is denoted as "ACC".

Table 5.1: Specifications for the X-band Nautical Radar Images.

Data set	Antenna Rotation Period (second)	Range Resolution (m/pixel)	Target Range (m)	Image Number
ACC1	1.31	7.51	1800-2500	172
ACC2	1.31	7.51	1800-2900	232
ACC3	1.31	7.51	900-2000	140
ACC4	1.31	7.51	900-1900	201
CRT1	2.10	7.51	1750-1950	283
CRT2	2.10	3.76	900-1150	173
CRT3	2.10	3.76	850-1100	139

5.1.2 GPS data

During the above trials, a GPS device was installed on the ship to collect the ship moving information for validating the tracking results of the proposed approaches.

The raw GPS data contains target position, speed and course. The raw GPS data is recorded in a format following the NMEA 0183 standard [73], which includes multiple sentences such as recommended minimum specific GPS data (GPRMC), geographic position - latitude/longitude (GPGLL), global positioning system fix data (GPGGA), course over ground and ground speed (GPVTG), time & date (GPZDA). Among these sentences, only the GPRMC sentence is used since it contains the required information for retrieving the target and velocities. In the GPRMC sentence, important parameters are delimited by comma and with the checksum in the end. For

example, the information contained in the GMRMC sentence `"$GPRMC,144738,A-,4717.3421,N,05359.5329,W,0.1,258.9,090310,20,W*5D"` is listed in Table 5.2.

Table 5.2: GPRMC Sentence.

Example	Name	Description
$GPRMC	Sentence identifier	GPS RMC header
144738	UTC time	hhmmss.sss
A	Data status	A = valid, V = warning
4717.3421	Latitude	ddmm.mmmm
N	N/S indicator	North/South latitude indicator
05359.5329	Longitude	ddmm.mmmmm
W	E/W indicator	East/West longitude indicator
0.1	Speed over ground	Target speed in knots
258.9	Course over ground	True course in degree
090310	Date	ddmmyy
20	Magnetic Variation	
W	E/W indicator	East/West indicator
*5D	Checksum	Covering previous values

Based on the retrieved coordinates (latitude and longitude) of the moving target and the measured coordinates of the fixed marine radar, the target range and bearing with respect to the radar can be calculated. The calculation of the great-circle distance between two points around the Earth's surface with respective latitudes and longitudes follows the Haversine formulas [74],

$$d = R \cdot c \tag{5.1}$$

$$c = 2 \arctan(\sqrt{a}, \sqrt{1-a}) \tag{5.2}$$

$$a = \sin^2(\Delta lat/2) + \cos(lat_1)\cos(lat_2)\sin^2(\Delta long/2) \tag{5.3}$$

where a is the square of half the chord length between two points, c is the angular distance in radian, R is the radius of the Earth(the mean radius value of 6731 km for the slightly ellipsoidal Earth), Δlab and $\Delta long$ are the latitude and longitude differences between the two points.

The bearing of the target can be calculated as [74]

$$\theta = \arctan(\sin(\Delta long)\cos(lat_2), \cos(lat_1)\sin(lat_2) - \sin(lat_1)\cos(lat_2)\cos(\Delta long)) \tag{5.4}$$

The complete target tracks of the trials ("ACC" and "CRT") are depicted in Fig. 5.1 and Fig. 5.3, respectively. The corresponding target kinematic parameters retrieved from the GPS data are shown in Fig. 5.2 and Fig. 5.4. These figures give an idea about the target moving modes. The seven radar image sequences used for tracking performance analysis are truncated data from these two trials.

5.2 Tracking Results

5.2.1 Parameter optimization for tracking filters

In order to validate the choice of the OS-CFAR for the KF based classical tracking approach, the detection performance of the OS-CFAR and CA-CFAR is compared in terms of P_d and P_{fa}. The experimental results using these two CFAR schemes from the datasets ACC1 and CRT1 are shown in Figs. 5.5-5.6. It can be found that the OS-CFAR outperforms the CA-CFAR detector since it can achieve higher probability of detection with the same probability of false alarm.

Moreover, the influence of the size of the OS-CFAR reference window on its detection performance is also investigated. From the P_d and P_{fa} curves (Fig. 5.7 and

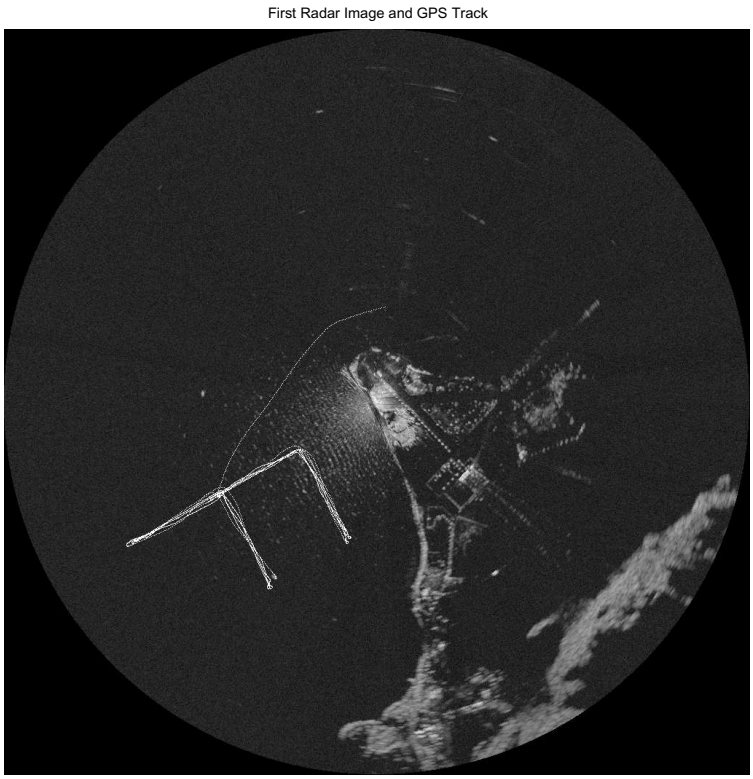

Figure 5.1: Complete target track during the ACC trial.

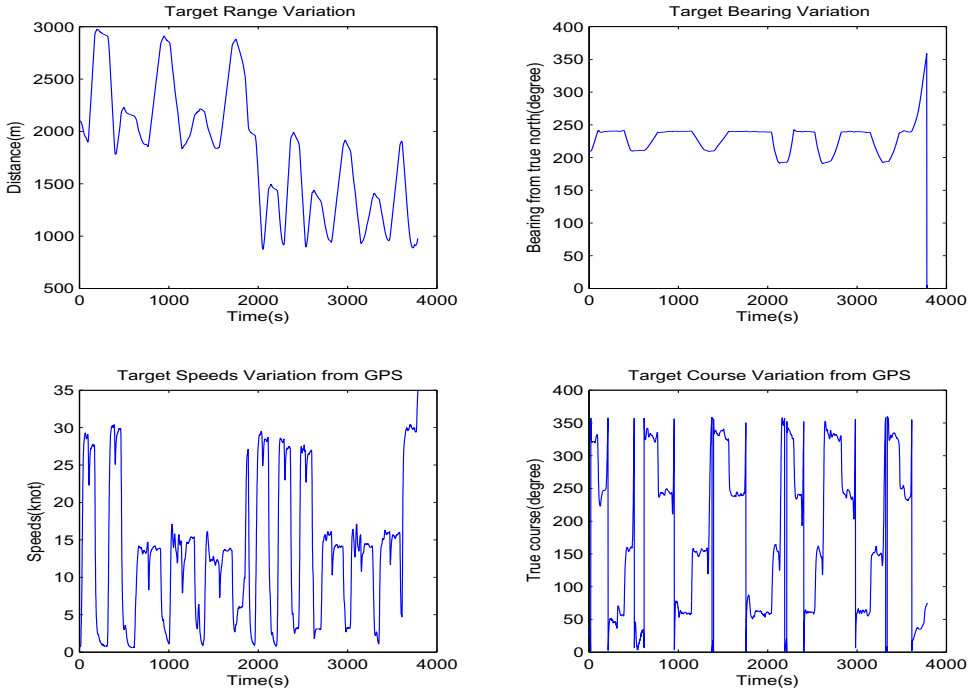

Figure 5.2: Variation of the target kinematic parameters during the ACC trial.

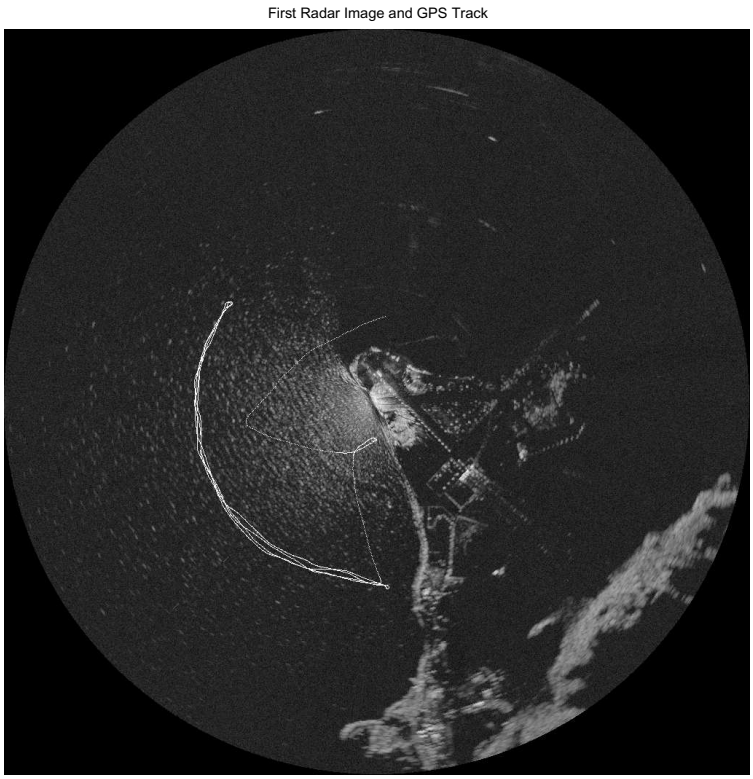

Figure 5.3: Complete target track during the CRT trial.

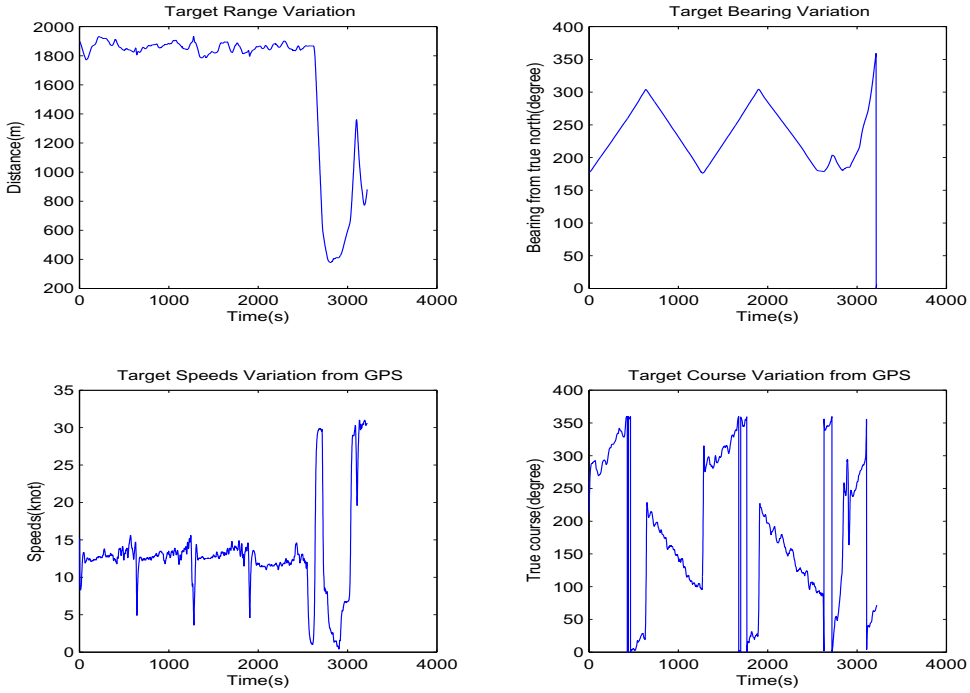

Figure 5.4: Variation of the target kinematic parameters during the CRT trial.

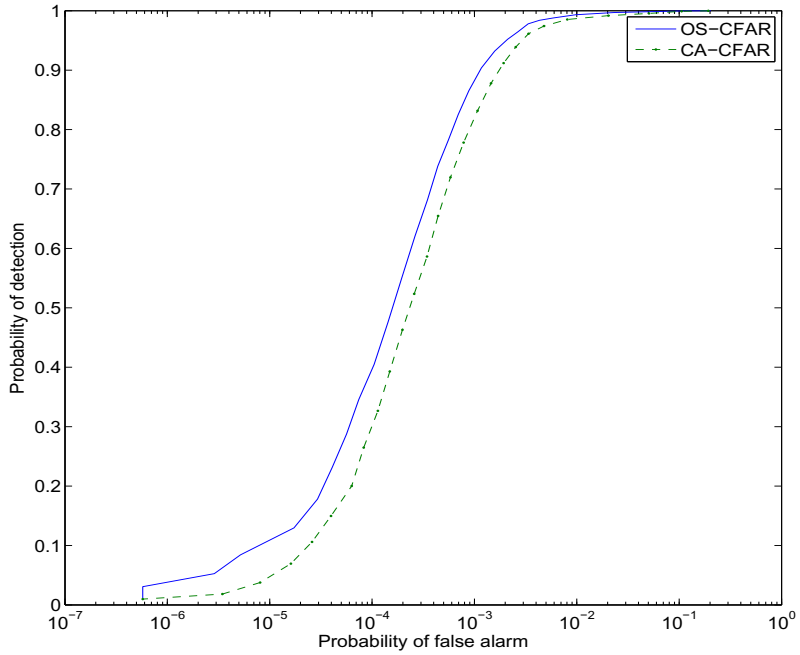

Figure 5.5: Comparison of P_d-P_{fa} curves of OS-CFAR and CA-CFAR from ACC1.

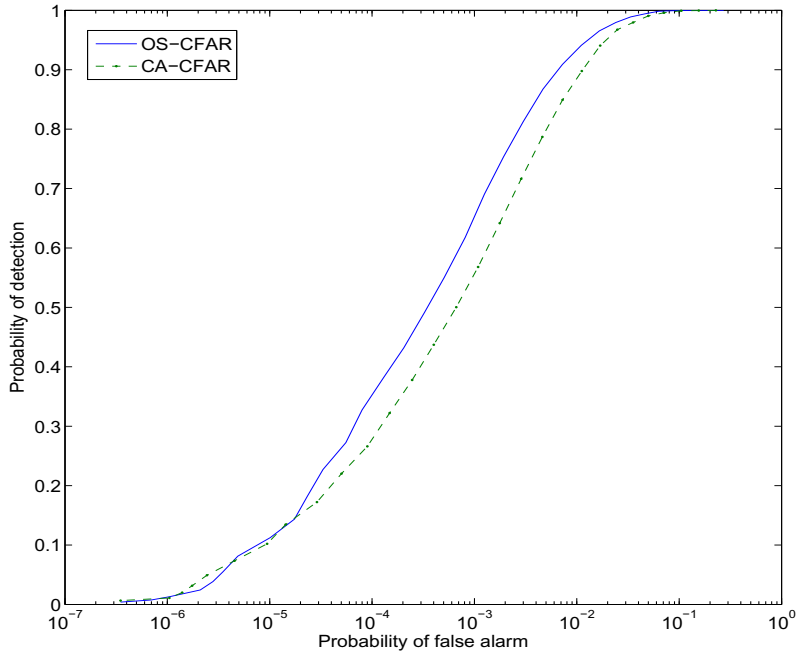

Figure 5.6: Comparison of P_d-P_{fa} curves of OS-CFAR and CA-CFAR from CRT1.

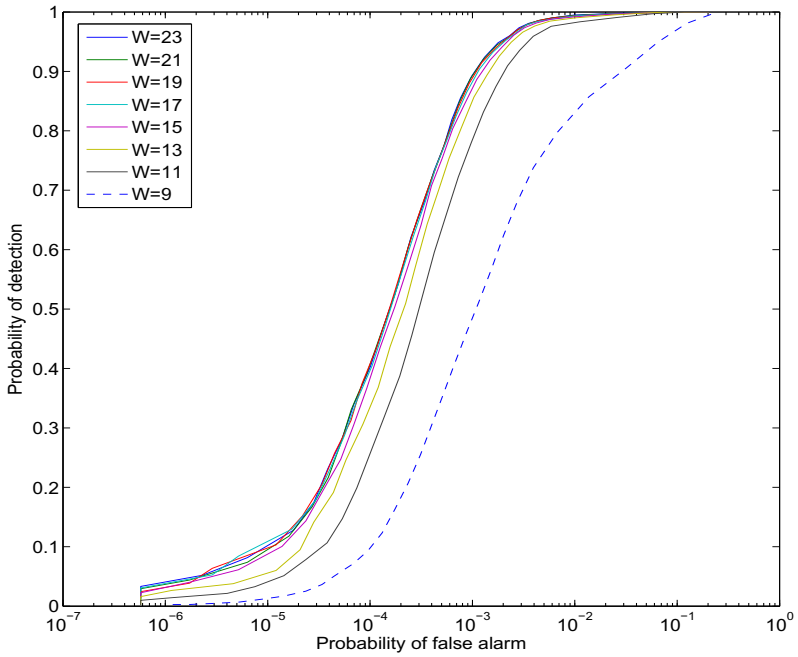

Figure 5.7: P_d-P_{fa} curves with different CFAR reference window sizes of OS-CFAR from ACC1.

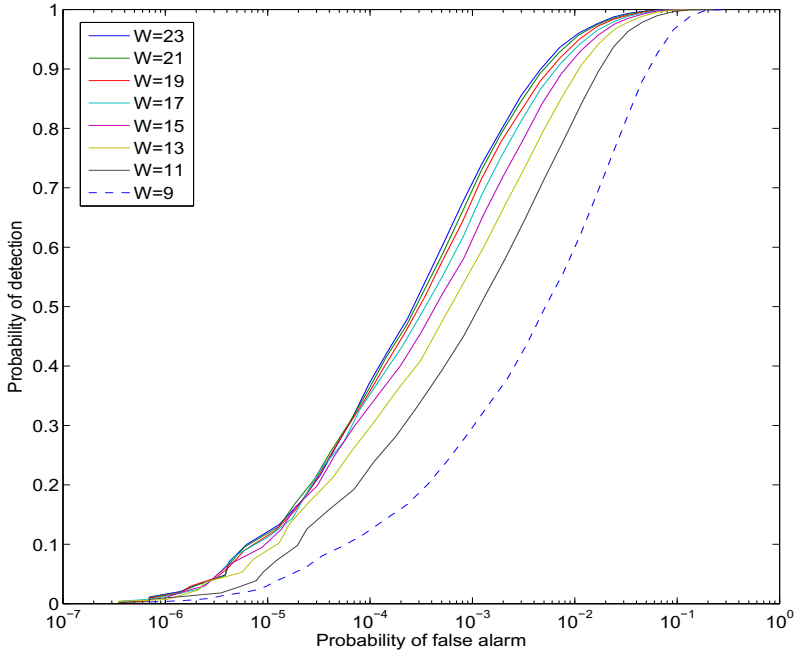

Figure 5.8: P_d-P_{fa} curves with different CFAR reference window sizes of OS-CFAR from CRT1.

Fig. 5.8) obtained from datasets ACC1 and CRT1, it can be found that increasing the CFAR reference window width W can improve the detection performance to some extent. However, if the reference window size is too large, the assumption of homogeneity for the reference cells will not be valid and a higher computational cost is required. On the other hand, it could also be shown that the effectiveness of the detection improvement due to the reference window size would be significantly decreased when the size reaches a certain value. As a result, the width and length W of the reference window are chosen as 21 pixels in the KF based classical tracking approach to achieve an acceptable detection performance with reasonable computational cost.

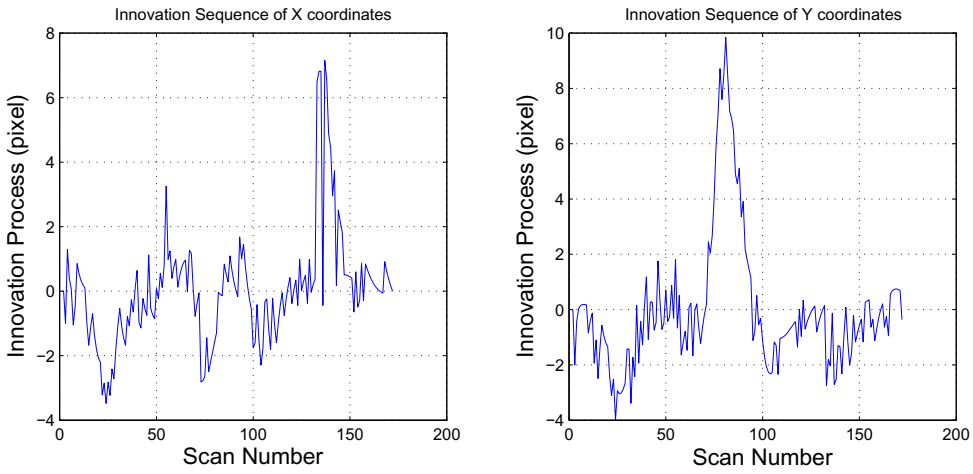

Figure 5.9: Innovation process without adaptive KF filtering from ACC1.

In order to validate the proposed innovation term based adaptive KF algorithm for maneuver, the variation of the innovation terms of the classical KF tracker are shown in Fig. 5.9 and Fig. 5.10 based on the results from the dataset ACC1, in which the target moves with a 90° abrupt turning. Fig. 5.9 shows the variation of the innovation term $\boldsymbol{\nu}_k$ along the x axis and y axis for the KF based tracking approach without the adaptive KF algorithm, while Fig. 5.10 shows the results of the approach using the adaptive KF algorithm. Comparison of these two figures shows that the

adaptive KF algorithm can effectively reduce the amplitude of KF innovation terms. Thus, the tracking performance can be improved as smaller innovation terms imply that estimated results are closer to practical results.

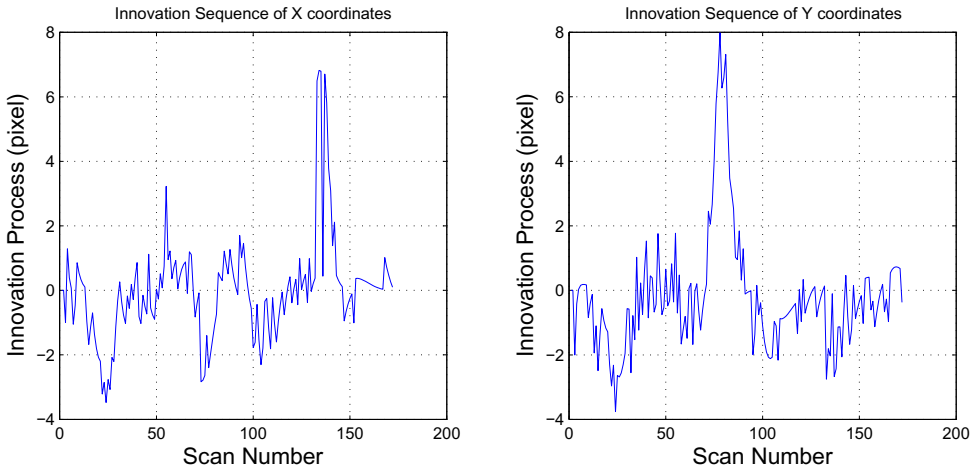

Figure 5.10: Innovation process with adaptive KF filtering from ACC1.

In order to determine the optimal values of the parameters used in the PF based visual tracking approaches, tracking performances are evaluated using the retrieved GPS data as the ground truth. Then, the root mean square error (RMSE) is employed to quantify the tracking accuracy. Here, the position RMSE is defined as

$$\text{RMSE} = \sqrt{\frac{1}{N}\sum_{i=1}^{N}\left((x_{1,i} - x_{2,i})^2 + (y_{1,i} - y_{2,i})^2\right)} \tag{5.5}$$

where $x_{1,i}$ and $y_{1,i}$ denote the estimated target coordinates using the particle filter based methods, $x_{2,i}$ and $y_{2,i}$ represent the reference target position coordinates from the GPS data, and N is the number of the target positions through an image sequence.

Generally, a larger number of PF samples would result in more accurate approximation of distributions in the Bayesian estimation, and more stable tracking performance. In order to investigate the influence of the number of PF samples on the tracking performance and computational cost, the variations of target position RMSE

and computational time against the PF sample numbers from dataset ACC1 are illustrated in Fig. 5.11 (a) and (b). It is clear that a large number of samples would stabilize the tracking performance, while the computational cost would increase nearly linearly with the increase of the number of samples. As a result, a proper number of samples should be determined to achieve an acceptable tracking performance with reasonable computational burden. In this thesis, number of samples N_s=300 is selected to assure stable tracking performances for the PF-KF based approach, while the number of samples for the PF-only based approach is set to 600.

Moreover, in order to verify the benefit of the enhanced reference target model (see Chapter 3) on the tracking performance, the tracking results using original and enhanced reference target models are also evaluated against the size of the square reference target region surrounding the target. More clutter will be included in the original reference target model when the size of the target region increases, which would undermine the tracking accuracy and stability. However, with the enhanced reference target model, good and stable tracking performance is secured with different sizes of the square reference regions (see Fig. 5.11(c)). Thus, this enhanced reference target model is adopted for both the PF-only and PF-KF based visual tracking approaches.

5.2.2 Tracking performance comparison

Among the seven available image sequences, datasets CRT1 and ACC1-4 are collected in a relatively low sea clutter environment, in which the target is relatively far from the radar. The tracking results, obtained by the classical approach (denoted as "CFAR-KF"), the PF-only based approach (denoted as "PF") and the combined PF-KF based approach (denoted as "PF-KF") from these images sequences, are illustrated as follows.

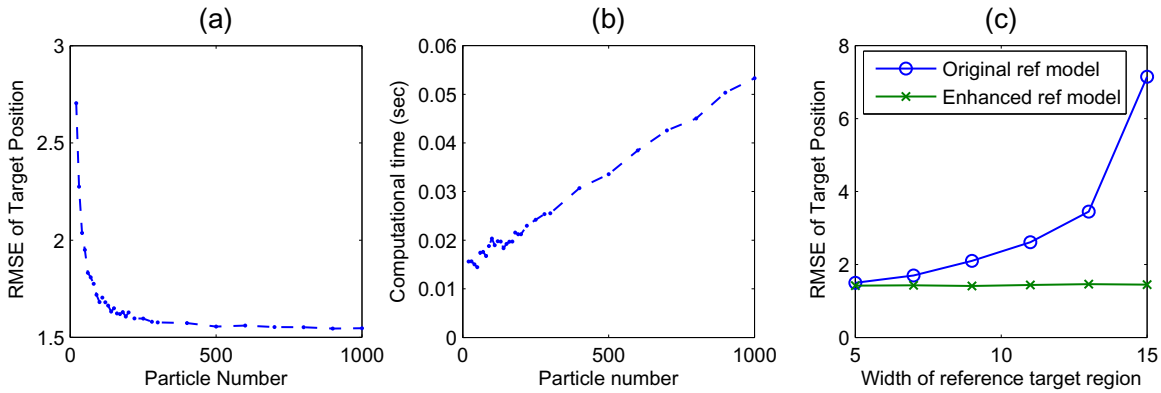

Figure 5.11: Tracking evaluation from CRT1: (a)Position RMSE against number of PF samples; (b)Computational time against number of PF samples; (c)Position RMSE against target region width using original and enhanced reference target models.

The tracking trajectories obtained from dataset CRT1 using the above three approaches are shown in Fig. 5.12, where the target was moving around the radar with a nearly constant speed and range. From the Figure, it can be found that the obtained trajectories agree well with that of the GPS data. The position RMSEs for these approaches are all approximately 2 pixels (15 m, also see Table 5.3). These values are considered to be acceptable as the size of the target is approximately 24 pixels in the radar image. Furthermore, from the states $x_k, y_k, \dot{x}_k, \dot{y}_k$, the target range ($\sqrt{(x_k - x_r)^2 + (y_k - y_r)^2}$, where x_r and y_r are the Cartesian radar position coordinates), bearing ($\pi/2 - \arctan((y_k - y_r)/(x_k - x_r))$), speed ($\sqrt{\dot{x}_k^2 + \dot{y}_k^2}$) and course ($\pi/2 - \arctan(\dot{y}_k/\dot{x}_k)$) can be derived. These derived target parameters are also compared with the raw GPS data as shown in Fig. 5.13. It can be found in Fig. 5.13 that the derived ship kinematic parameters using the three tracking approaches all agree fairly well with the GPS data.

For the dataset ACC1, where the target moved with an acceleration at the beginning, then a 90° sharp turn, and a deceleration in the end, the tracking trajectories and variations of kinematic parameters are illustrated in Fig. 5.14 and Fig. 5.15,

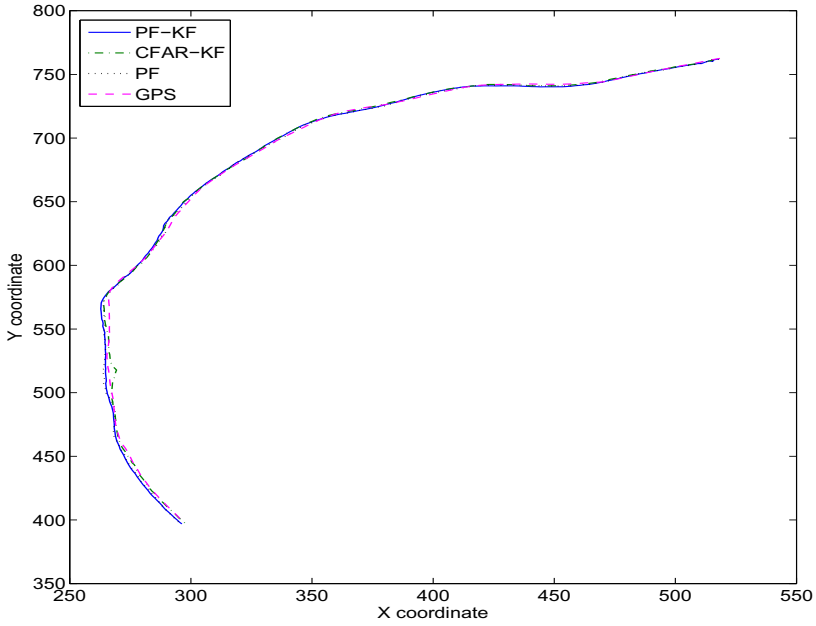

Figure 5.12: Target tracks obtained by CFAR-KF, PF, PF-KF estimation and GPS from CRT1.

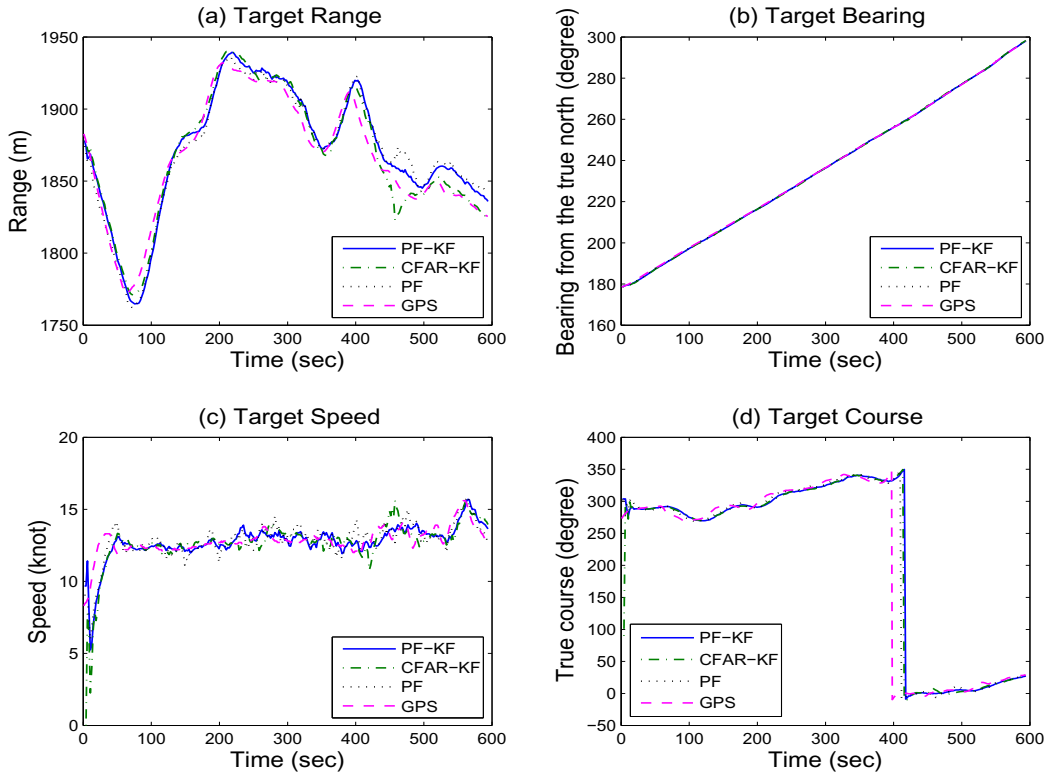

Figure 5.13: Variations of target information obtained by CFAR-KF, PF, PF-KF estimation and GPS from CRT1: (a)Target range; (b)Target bearing; (c)Target speed; (d)Target course.

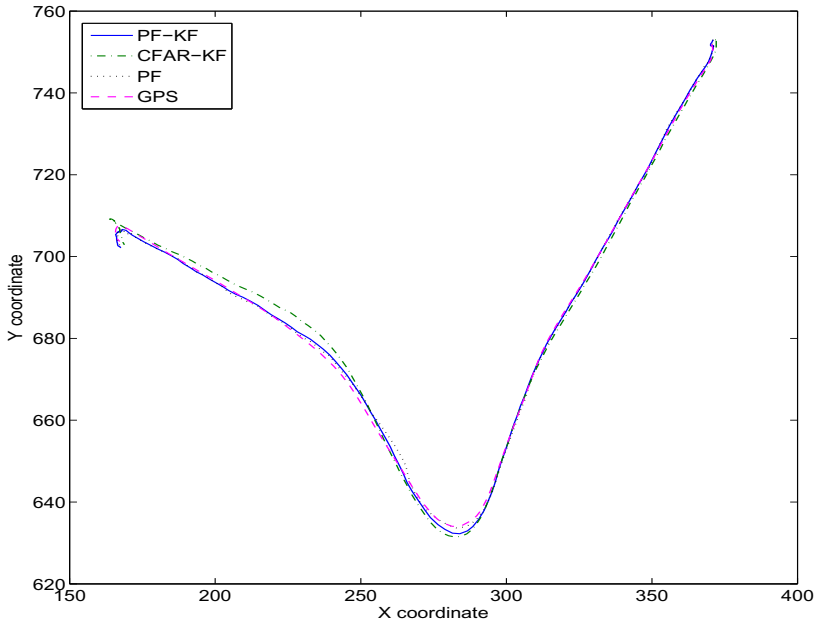

Figure 5.14: Target tracks obtained by CFAR-KF, PF, PF-KF estimation and GPS from ACC1.

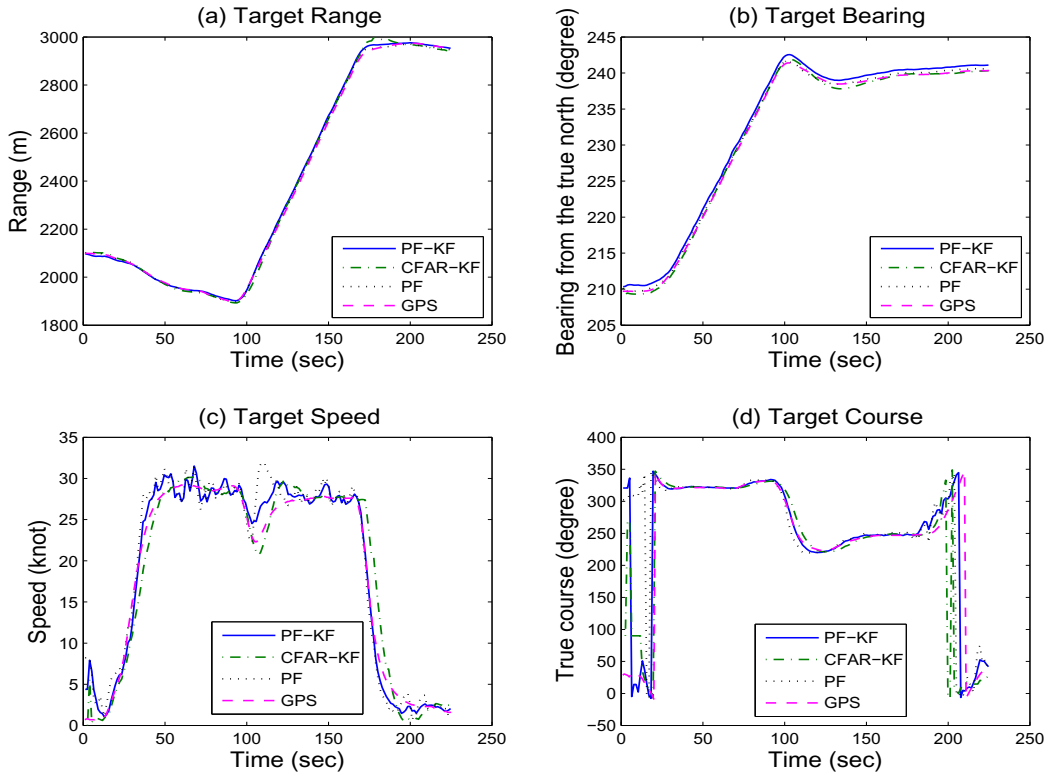

Figure 5.15: Variations of target information obtained by CFAR-KF, PF, PF-KF estimation and GPS from ACC1: (a)Target range; (b)Target bearing; (c)Target speed; (d)Target course.

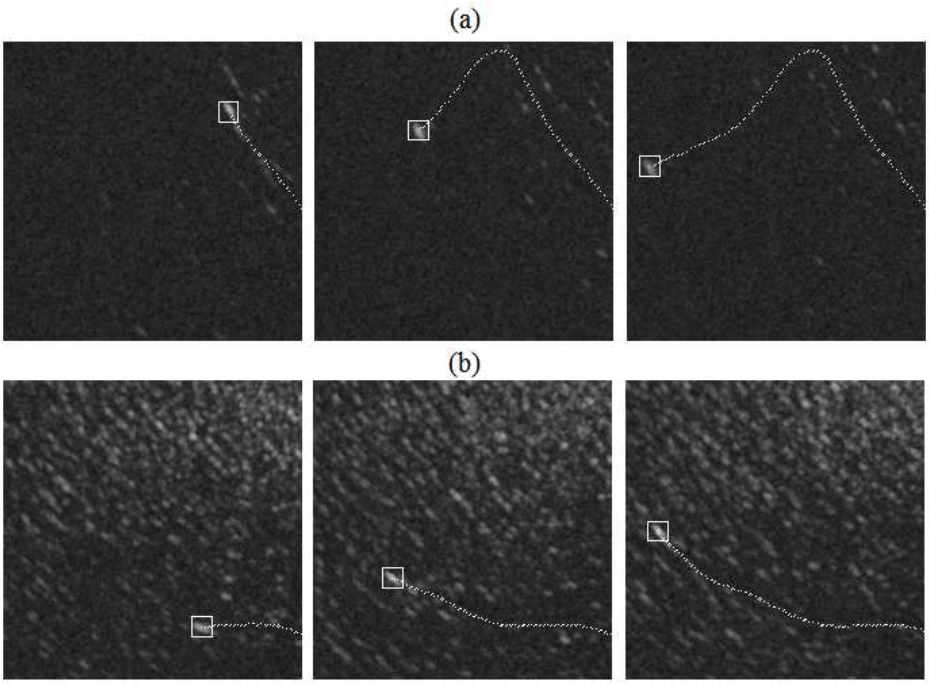

Figure 5.16: PF-KF estimated target with trajectory history in frame 60, 100, 120 for: (a)ACC1; (b)CRT1.

respectively. From Fig. 5.15 and the RMSE values of the kinematic parameters in Table 5.3, it can be found that all the three approaches can obtain similar tracking accuracy in target position estimation. However, the PF-only based approach performs worse in the target velocity estimation than the classical KF-based approach and the PF-KF based approach. In Fig. 5.15 (c), the speed curve obtained by the "PF" approach shows large deviation from the GPS result. Thus, the PF-only based visual tracking approach may not work well for tracking maneuvering target. In order to show the results more clearly, Fig. 16 depicts selected frames showing tracked target marked with a white box from datasets ACC1 and CRT1. In conclusion, it is found the performances of the "PF-KF", "PF" and "CFAR-KF" methods are similar due to low sea clutter from the above results.

Similar tracking results can be found from datasets ACC2-4 (see Figs. 5.17-5.22), in which the target motion also contains a 90° turning, an acceleration (and/or a

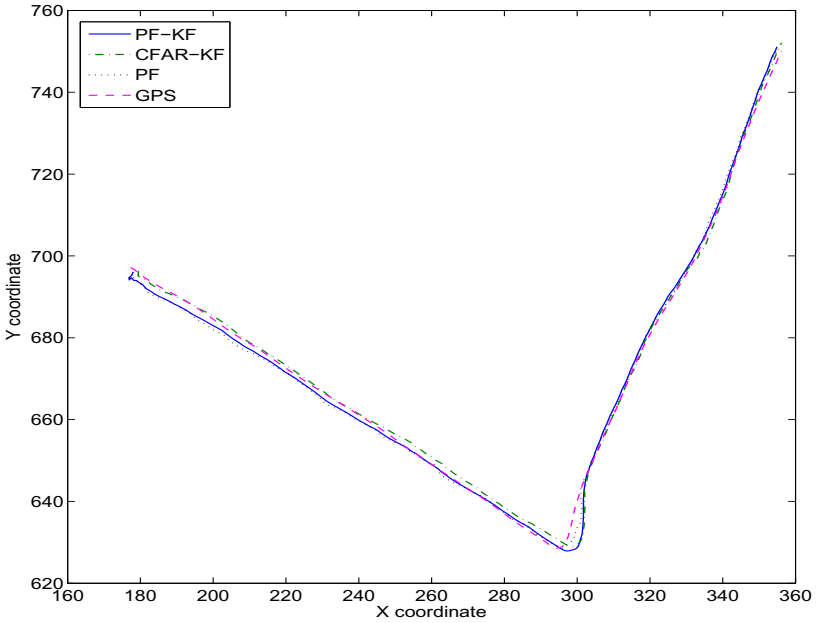

Figure 5.17: Target tracks obtained by CFAR-KF, PF, PF-KF estimation and GPS from ACC2.

deceleration). The only difference of these datasets is that the target motion changes happened at different ranges. From these datasets, all the three methods can obtain a fairly good position estimation (including the derived range and bearing estimation). However, the KF based classical approach ("CFAR-KF") and the proposed PF-KF based approach ("PF-KF") perform better than the proposed PF-only based approach ("PF") in velocity estimation.

Under strong clutter background, the tracking performance of the proposed visual tracking approaches and classical approach degrade since more false target signals are detected or real target signals are lost due to the decrease of discrimination between the target and clutter signals. In order to analyze the performance of the proposed method under strong clutter environment, the CRT2 and CRT3 sequences, in which targets are about 850-1150 meters away from the radar and surrounded by quite strong clutter, are tested.

The tracking results from CRT2 are depicted in Figs. 5.23-5.24, from which it can

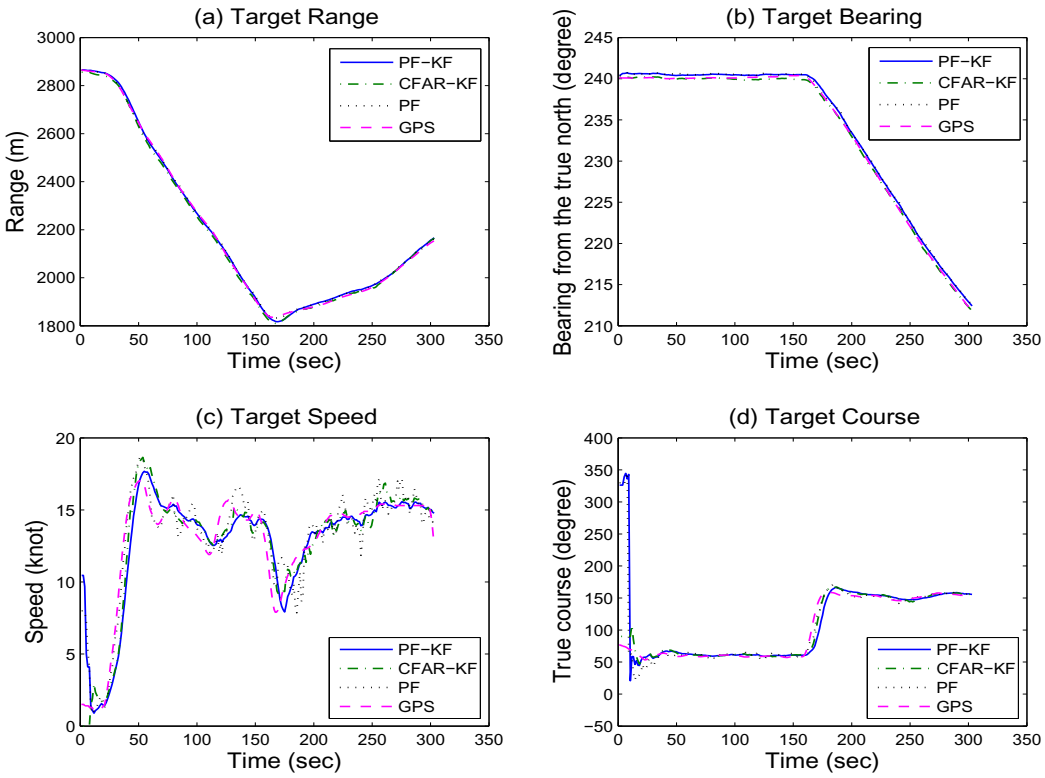

Figure 5.18: Variations of target information obtained by CFAR-KF, PF, PF-KF estimation and GPS from ACC2: (a)Target range; (b)Target bearing; (c)Target speed; (d)Target course.

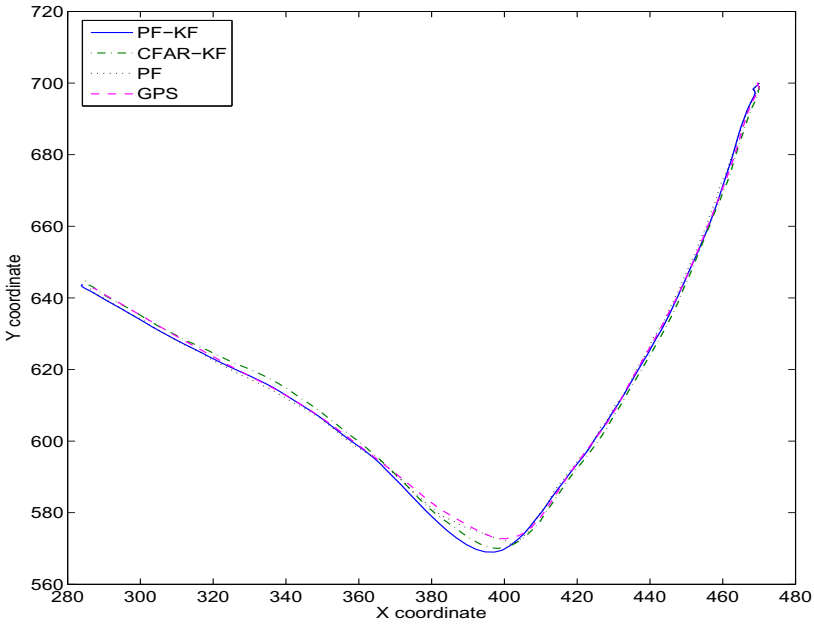

Figure 5.19: Target tracks obtained by CFAR-KF, PF, PF-KF estimation and GPS from ACC3.

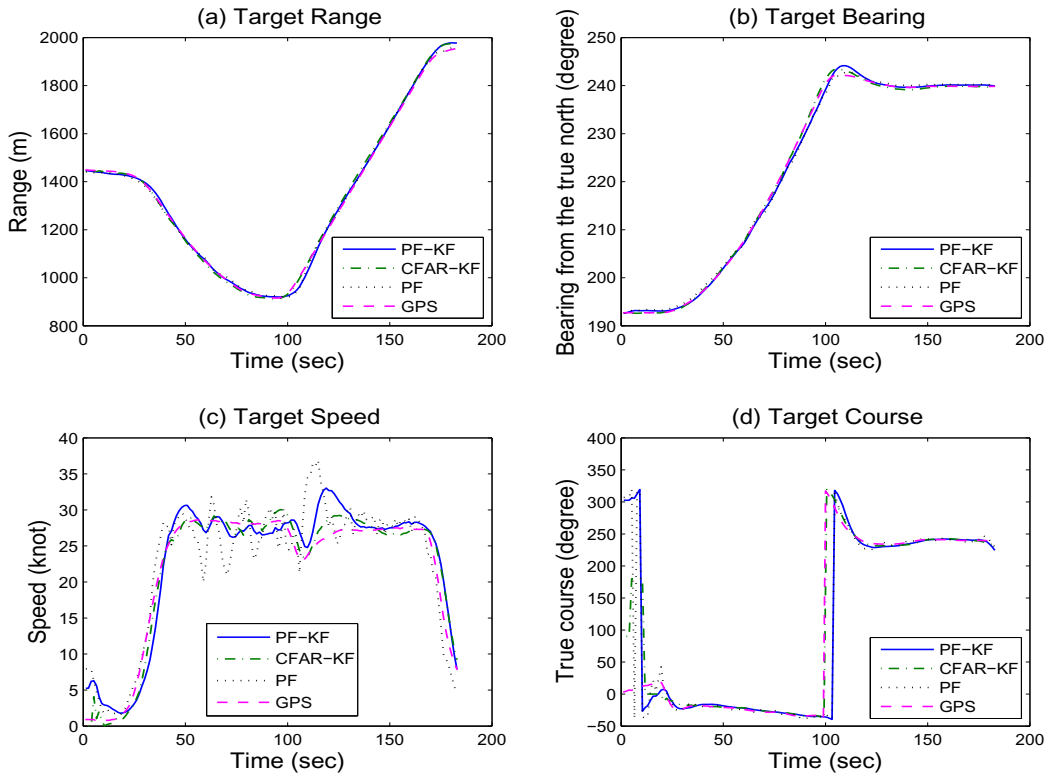

Figure 5.20: Variations of target information obtained by CFAR-KF, PF, PF-KF estimation and GPS from ACC3: (a)Target range; (b)Target bearing; (c)Target speed; (d)Target course.

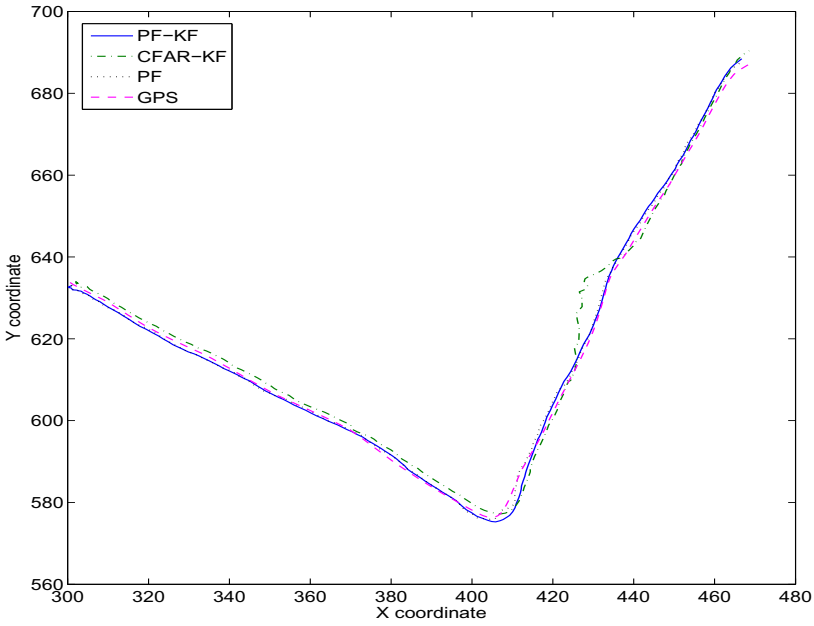

Figure 5.21: Target tracks obtained by CFAR-KF, PF, PF-KF estimation and GPS from ACC4.

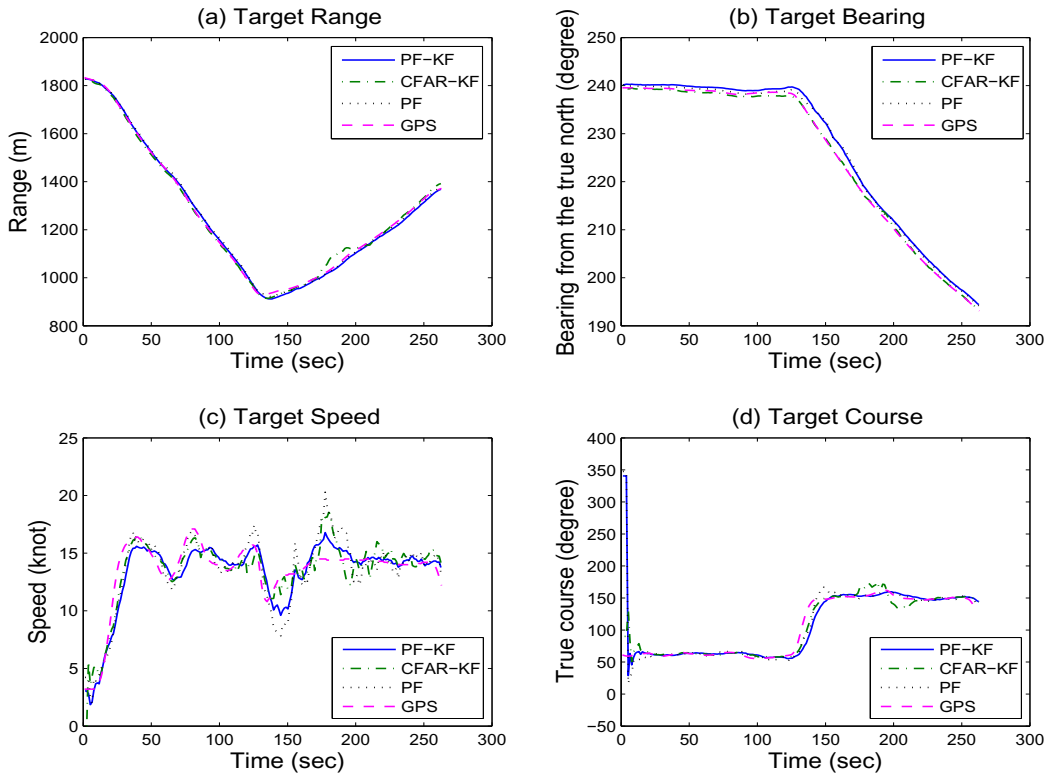

Figure 5.22: Variations of target information obtained by CFAR-KF, PF, PF-KF estimation and GPS from ACC4: (a)Target range; (b)Target bearing; (c)Target speed; (d)Target course.

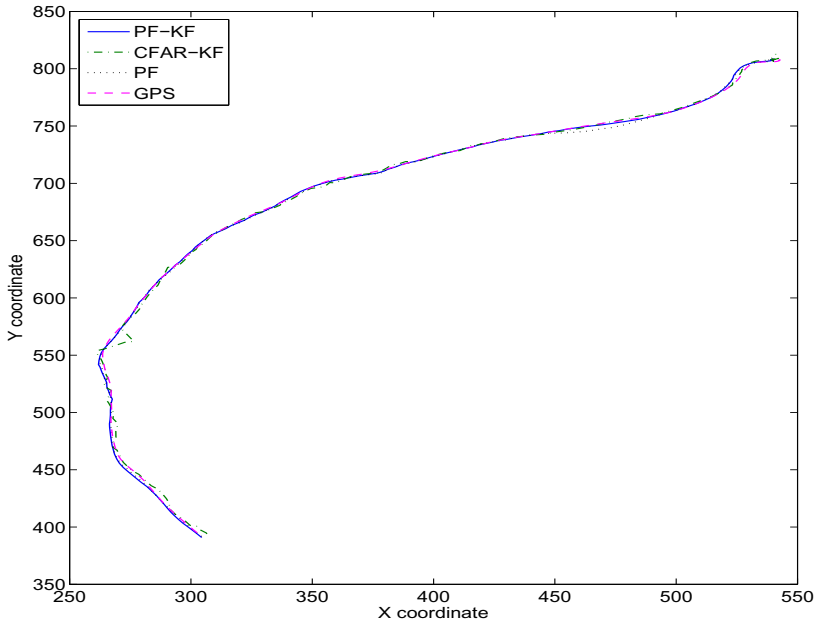

Figure 5.23: Target tracks obtained by CFAR-KF, PF, PF-KF estimation and GPS from CRT2.

Table 5.3: Comparison of target parameters RMSE obtained by CFAR-KF, PF and PF-KF from ACC1-4 and CRT1.

Data sets	Approach	Position (pixel)	Range (m)	Speed (knot)	Bearing (degree)	Course (degree)
ACC1	CFAR-KF	2.57	19.7	1.65	0.87	16.0
ACC1	PF	1.64	17.1	2.63	0.64	18.9
ACC1	PF-KF	1.54	21.1	1.91	0.19	10.8
ACC2	CFAR-KF	2.05	20.3	1.23	1.44	6.30
ACC2	PF	1.76	12.6	1.38	0.88	8.47
ACC2	PF-KF	1.70	14.2	1.71	0.90	9.35
ACC3	CFAR-KF	2.40	15.7	1.36	0.47	5.34
ACC3	PF	2.40	12.6	3.60	0.73	5.56
ACC3	PF-KF	1.77	13.7	2.60	0.63	8.82
ACC4	CFAR-KF	2.15	17.2	1.22	0.99	7.85
ACC4	PF	2.99	10.2	1.67	0.91	7.43
ACC4	PF-KF	2.11	8.34	1.43	0.90	9.73
CRT1	CFAR-KF	1.80	7.56	1.25	0.35	5.99
CRT1	PF	1.56	11.0	1.07	0.26	5.16
CRT1	PF-KF	1.53	10.5	1.05	0.27	6.41

Table 5.4: Comparison of target parameters RMSE obtained by CFAR-KF, PF and PF-KF from CRT2-3.

Data sets	Approach	Position (pixel)	Range (m)	Speed (knot)	Bearing (degree)	Course (degree)
CRT2	CFAR-KF	3.75	7.36	1.70	0.71	13.5
CRT2	PF	2.42	5.88	1.10	0.54	8.56
CRT2	PF-KF	2.04	4.22	0.81	0.40	10.8
CRT3	CFAR-KF	-	-	-	-	-
CRT3	PF	4.01	9.50	2.16	0.96	11.6
CRT3	PF-KF	3.89	6.03	1.53	0.81	7.39

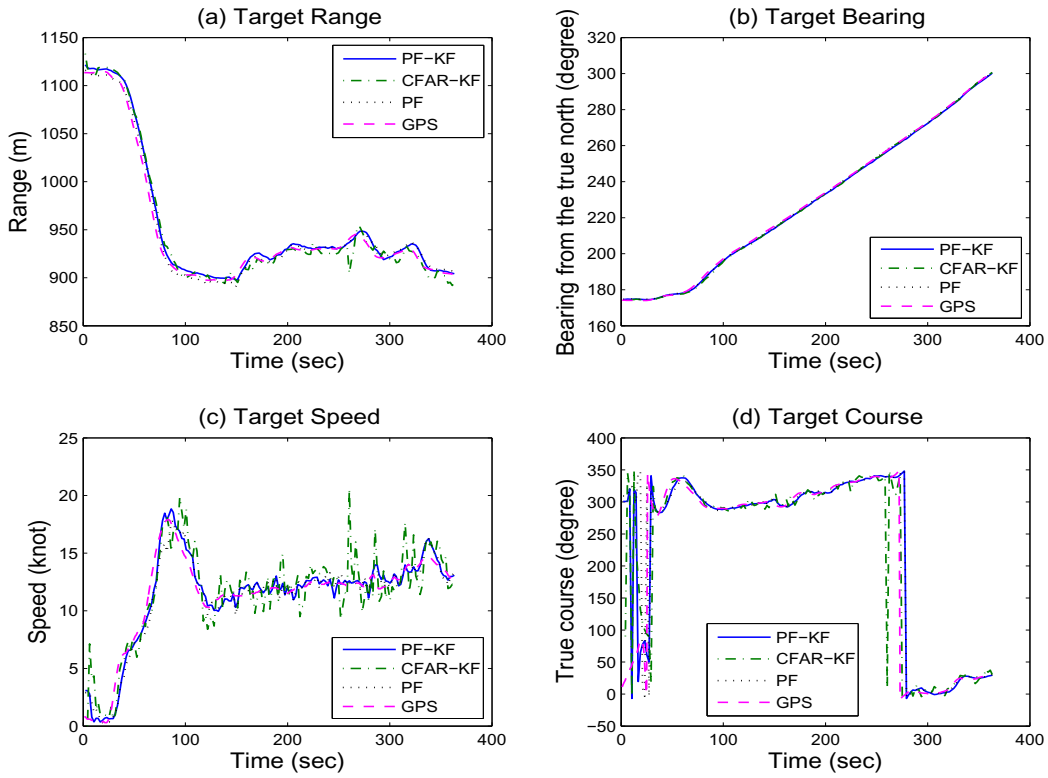

Figure 5.24: Variations of target information obtained by CFAR-KF, PF, PF-KF estimation and GPS from CRT2: (a)Target range; (b)Target bearing; (c)Target speed; (d)Target course.

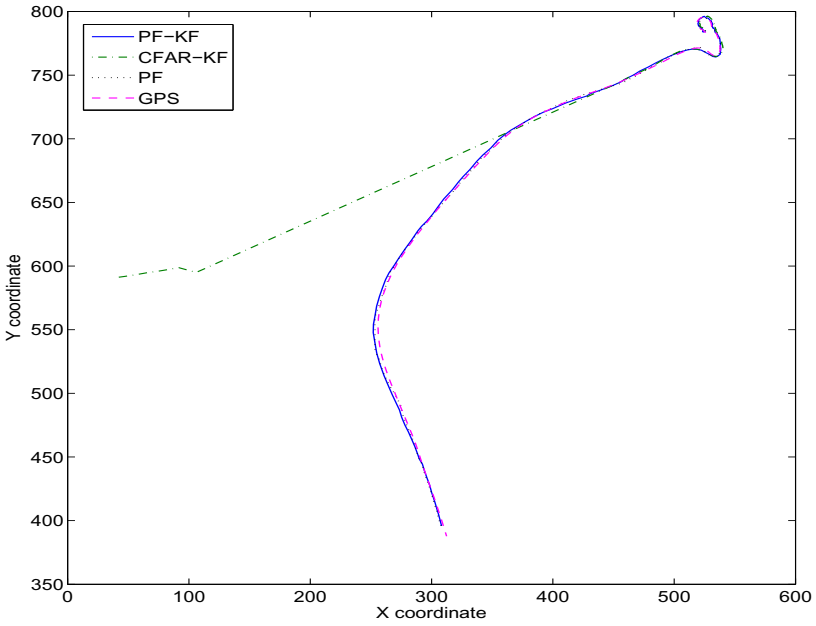

Figure 5.25: Target tracks obtained by CFAR-KF, PF, PF-KF estimation and GPS from CRT3.

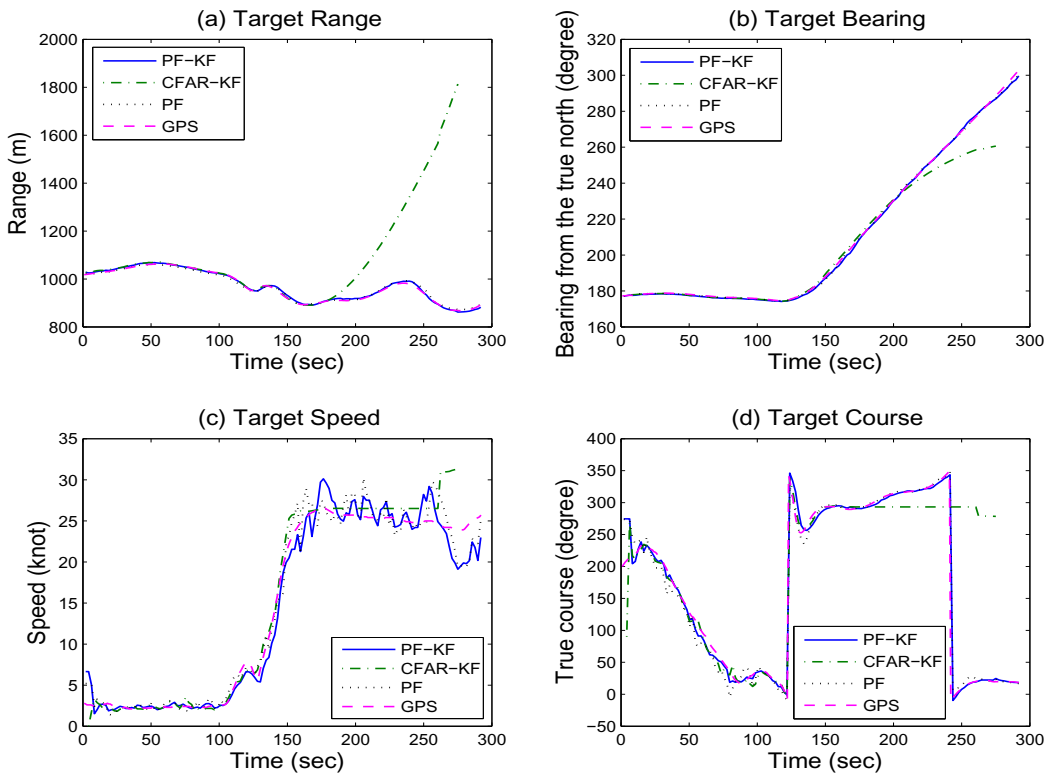

Figure 5.26: Variations of target information obtained by CFAR-KF, PF, PF-KF estimation and GPS from CRT3: (a)Target range; (b)Target bearing; (c)Target speed; (d)Target course.

be seen that the proposed visual tracking approaches show better tracking performance than the classical approach. Especially in the later part of the dataset CRT2 (scans 100-173, or 210-363 seconds), the position RMSE is large as 6 pixels using the classical approach, but less than 2 pixels with the proposed visual approaches. From the CRT3 estimation results shown in Figs. 5.25-5.26, it is found that the classical approach even fails to detect the target in several consecutive images due to the high clutter background and fails to provide correct track, while the proposed PF-only and PF-KF based visual tracking approaches are still able to generate a satisfactory track but with a larger position RMSE ($\approx$ 4 pixels). More detailed statistics of tracking results with the proposed "PF-KF" approach, "PF" approach and the classical "CFAR-KF" approach are listed in Table 5.4, from which the proposed PF-KF based

approach is also shown to outperform the PF-only based approach and classical approach in the estimation accuracy of the target position and velocity. Although the performances of the PF-KF, PF and CFAR-KF methods degrade under strong sea clutter, the superiority of the PF-KF based approach is more obvious. It should be noted that the GPS data is considered to be ground truth with error in this thesis. The interpretation of the experimental results are based on the comprehensive analysis of the RMSE errors of different kinematic parameters and tracking trajectories.

Under relatively weak sea clutter, the "PF-KF" approach performs similarly to the classical "CFAR-KF" approach in tracking accuracy of target position and velocity. From the above analysis on the seven datasets, it is also found that the PF-only based approach performs worse in the velocity estimation when the target maneuvers more often. When the sea clutter is relatively strong, the proposed PF-KF and PF-only based visual tracking approaches outperform the classical KF based approach.

Chapter 6

Conclusion and Future Work

6.1 Conclusion

For maneuvering target tracking from X-band nautical radar images, two particle filter based visual tracking approaches are designed to automatically obtain the target position and velocity in this thesis: a PF-only based approach and a combined particle-Kalman filters (PF-KF) based approach. Moreover, a Kalman filter based classical tracking approach is also presented in order to evaluate the tracking performance of the proposed PF based algorithms. These three tracking approaches have been tested in seven practical X-band radar image sequences, which are collected under different radar parameters, different target moving modes, and different sea clutter environments.

In developing the KF based classical tracking approach, the OS-CFAR processing is first employed for detecting target signals since it shows better detection performance than the CA-CFAR. Then, the Kalman filter is used for recursively estimating the target position and velocity as the optimal solution to a constructed linear and Guassian tracking system. This linear-Gaussian system employs the measured

target center coordinates along the x and y axis of the scan converted radar images as the measurements, and a constant acceleration motion model as the state transition function. Moreover, an adaptive KF algorithm is also integrated into the KF-based approach to deal with target maneuvering. It is shown that the designed KF-based classical tracking approach can effectively track the target with different moving modes, under relatively weak sea clutter environments. However, the tracking performance of the KF-based classical tracking approach would degrade significantly when the sea clutter becomes relatively strong.

In order to address this problem, a visual tracking method is first integrated into the SIR particle filter framework to track the maneuvering target from the nautical radar images. This PF-only based visual tracking strategy employs the kernel-based histogram model to represent the target, and Bhattacharyya coefficient based distance to provide the likelihood function for particle filtering. It is found the kernel-based histogram target model is relatively robust to the change of target's pose and scale, and is computationally efficient. The kernel function helps locate an accurate target center position. The Bhattacharyya coefficient based distance can provide a suitable metric for target position and velocity estimation by the PF. As the accuracy of the reference target model is critical to the tracking accuracy and stability of the PF based algorithm, the modifications made on the reference target model, including the automatic reference target model initialization, enhanced target model construction, and updating reference model, can effectively improve the tracking accuracy, stability and flexibility.

As the particle filter usually requires high computational cost, which is closely related to the number of the samples for particle filtering, a combined PF-KF based visual tracking approach is further proposed. The combined PF-KF procedure reduces the dimension of state vector for PF sampling, which can effectively reduce the risk

of tracking divergence and reduce the computational cost. The modifications of the reference target model is also integrated. The automatic reference model initialization helps improve the flexibility of the tracking algorithm. The enhanced reference target model construction can improve the tracking stability. The updating reference target model can deal with possible target's appearance change through the tracking process although the change in this experiment is slow. Moreover, the adaptive KF algorithm that is integrated into the combined PF-KF method can effectively improve the tracking accuracy and stability when target maneuvers.

Based on the test using field nautical radar data which accounts for different radar parameters, different target moving modes, and different sea clutter background, it is found that the PF-KF based visual tracking can outperform the PF-only based visual tracking approach in velocity estimation, and outperform the KF based classical tracking approach when the sea clutter is quite strong. In conclusion, through the experiment with practical field data, the proposed PF-KF based visual tracking approach can reliably and effectively estimate position and velocity of a maneuvering target directly based on the nautical radar images.

6.2 Future Work

In this thesis, the proposed PF-KF visual tracking approach is only designed for single target tracking and tested in the available nautical radar image sequences collected under certain radar configurations and environments. In the future, this approach needs to be improved to address the multiple targets tracking problem. More practical nautical radar data can be used to test the robustness and performance of the tracking algorithm. In order to deal with target tracking under more complicated situation, more sophisticated visual tracking algorithms (e.g., MIL tracking, VTD, and

Ensemble Tracking) may be considered in the future work. Moreover, the approximate initial target position is assumed to be available before tracking, an algorithm for automatically detecting the initial target should be designed and integrated into the proposed algorithm in the future.

Bibliography

[1] A. Farina and F.A. Studer, *Radar Data Processing, Volume 1-Introduction and Tracking*, Research Studies Press, England, 1985.

[2] R. Khan, B. Gamberg, D. Power, J. Walsh, B. Dawe, W. Pearson, and D. Millan, "Target detection and tracking with a high frequency ground wave radar," *IEEE J. Ocean. Eng.*, vol. 19, no. 4, pp. 540-548, Oct. 1994.

[3] J.N. Briggs, *Target Detection By Marine Radar*, Institution of Electrical Engineers, 2004.

[4] R.Q. Robe, D.F. Paskausky, and G.L. Hover, "Performance of Coast Guard medium range surveillance (MRS) aircraft radars in search and rescue (SAR) missions," *Proc. OCEANS '88. A Partnership of Marine Interests*, vol.4, pp. 1448-1453, Nov. 1988.

[5] C. Onunka and G. Bright, "Autonomous marine craft navigation: On the study of radar obstacle detection," *Int. Conf. Control Automation Robotics & Vision (ICARCV)*, pp. 567-572, Dec. 2010.

[6] Canadian Coast Guard vessel tracffic services in Pacific region. `http://www.ccg-gcc.gc.ca/e0003910`.

[7] S. Giompapa, F. Gini, A. Farina, A. Graziano, R. Croci, and R. DiStefano, "Maritime border control multisensor system," *IEEE Aerosp. Electron. Syst. Mag.*, vol. 24, no. 8, pp. 9-15, Aug. 2009.

[8] A. Dzvonkovskaya, K.W. Gurgel, H. Rohling, and T. Schlick, "Low power high frequency surface wave radar application for ship detection and tracking," *Proc. IEEE Radar Conf.*, pp. 627-632, Sep. 2008.

[9] M. Skolnik, *Radar Handbook*, 2nd ed., McGraw-Hill, New York, 1990.

[10] S. Tay, A. Coatanhay, F. Maussang, and R. Garello, "A tracking algorithm for GNSS reflected signals on sea surface," *IEEE Int. Conf. Geoscience and Remote Sensing Symposium (IGARSS)*, pp. 3821-3824, Jul. 2010.

[11] C. Xiao and H. Cha, "Application of time-frequency distribution to target detecting in sea clutter," *Int. Conf. Image and Information Processing (ICIIP)*, vol. 46, pp. 112-116, 2012.

[12] G. Hennessey, H. Leung, A. Drosopoulos, and P.C. Yip, "Sea-clutter modeling using a radial-basis-function neural network," *IEEE J. Ocean. Eng.*, vol. 26, no. 3, pp. 358-372, Jul. 2001.

[13] P.P. Gandhi and S. Kassam, "Analysis of CFAR processors in nonhomogeneous background", *IEEE Trans. Aerosp. Electron. Syst.*, vol.24, no.4, pp.427-445 Jul. 1988.

[14] G. B. Goldstein, "False-alarm regulation in log-normal and Weibull clutter", *IEEE Trans. Aerosp. Electron. Syst.*, vol.9, no. 1, pp. 84-92, Jan. 1973.

[15] S. Watts, "Radar sea clutter modelling and simulation - recent progress and future challenges," *Radar Clutter Modelling, IET Seminar*, pp. 1-7, Feb. 2008.

[16] T. Thayaparan and S. Kennedy, "Detection of a manoeuvring air target in sea-clutter using joint time-frequency analysis techniques," *IET Proc. Radar, Sonar and Navigation*, vol. 151, no. 1, pp. 19-30, Feb. 2004.

[17] M. Dakovic, T. Thayaparan, and L. Stankovic, "Time-frequency-based detection of fast manoeuvring targets," *IET Signal Processing*, vol. 4, no. 3, pp. 287-297, Jun. 2010.

[18] G. Wang, X. Xia, B.T. Root, V.C. Chen, Y. Zhang, and M. Amin, "Manoeuvring target detection in over-the-horizon radar using adaptive clutter rejection and adaptive chirplet transform," *IEE Proc. Radar, Sonar and Navigation*, vol. 150, no. 4, pp. 292-298, 1 Aug. 2003.

[19] P. Wu, J. Wang, and W. Wang, "A novel method of small target detection in sea clutter," *ISRN Signal Processing*, vol. 2011, Article ID 651790, 10 pages, 2011.

[20] D.E. Rumelhart, J.L. McClelland, and PDP Research Group, *Parallel Distributed Processing: Explorations in the Microstructure of Cognition, vol. 1: Foundations*, MIT Press, Cambridge, MA, USA, 1986.

[21] S. Haykin, *Neural Networks. A Comprehensive Foundation.* 2nd ed. London, UK, Prentice-Hall, 1999.

[22] R. Vicen-Bueno, R. Carrasco-Alvarez, M.P. Jarabo-Amores, J.C. Nieto-Borge, and M. Rosa-Zurera, "Ship detection by different templates and multilayer perceptrons from incoherent maritime radar data," *IET Radar, Sonar and Navigation*, vol. 5, no. 2, pp. 144-154, May 2011.

[23] H. Leung, G. Hennessey, and A. Drosopoulos, "Signal detection using the radial basis function coupled map lattice," *IEEE Trans. Neural Netw.*, vol. 11, no. 5, pp. 1133-1151, Sep. 2000.

[24] G. Lopez-Risueno, J. Grajal and R. Diaz-Oliver, "Target detection in sea clutter using convolutional neural networks," *Proc. IEEE Radar Conf.*, pp.321-328, May 2003.

[25] Y. Boers and J.N. Driessen, "Particle filter based detection for tracking," *Proc. American Control Conf.*, pp. 4393-4397, Jun. 2001.

[26] R.E. Kalman, "A new approach to linear filtering and prediction problems," *Transactions of the ASME, Ser. D, Journal of Basic Engineering*, no. 82, pp. 34-45, 1960.

[27] S. Haykin, *Kalman Filtering and Neural Networks*, Wiley-Interscience, Sep. 2001.

[28] S.J. Julier and J.K. Uhlmann, "A new extension of the Kalman filter to nonlinear system," *Proc. SPIE*, vol. 3068, pp. 182-193, 1997.

[29] S.S. Blackman, *Multiple-Target Tracking with Radar Applications*, Artech House, Dedham, 1986.

[30] Y. Bar-Shalom, *Multitarget-Multisensor Tracking: Applications and Advances, Vol. II*, Artech House, Norwood, 1992.

[31] M.S. Arulampalam, S. Maskell, N. Gordon, and T. Clapp, "A tutorial on particle filters for online nonlinear/non-Gaussian Bayesian tracking," *IEEE Trans. Signal Proces.*, vol. 50, no. 2, pp. 174-188, Feb. 2002.

[32] N.J. Gordon, D.J. Salmond, and A.F.M. Smith, "Novel approach to nonlinear/non-Gaussian Bayesian state estimation," *IEE Proc.-F*, vol. 140, no.2, pp. 107-113, Apr. 1993.

[33] F. Gustafsson, F. Gunnarsson, N. Bergman, U. Forssell, J. Jansson, R. Karlsson, and P.J. Nordlund, "Particle filters for positioning, navigation, and tracking," *IEEE Trans. Signal Proces.*, vol. 50, no. 2, pp. 425-437, Feb. 2002.

[34] S.K. Zhou, R. Chellappa, and B. Moghaddam, "Visual tracking and recognition using appearance-adaptive models in particle filters", *IEEE Trans. Image Process.*, vol. 13, no. 11, pp. 1491-1506, Nov. 2004.

[35] G. Kitagawa, "Monte Carlo filter and smoother for non-Gaussian nonlinear state space models," *Comput. Graph. Statist.*, vol. 5, no. 1, pp. 1-25, 1996.

[36] M. Pitt and N. Shephard, "Filtering via simulation: auxiliary particle filters," *J. Amer. Statist. Assoc.*, vol. 94, no. 446, pp. 590-599, 1999.

[37] J. Liu, W. Wang, and F. Ma, "A regularized auxiliary particle filtering approach for system state estimation and battery life prediction," *Smart Materials and Structures*, vol. 20, no. 7, pp. 1-9, 2011.

[38] C. Musso, N. Oudjane, and F. LeGland, "Improving regularised particle filters," in *Sequential Monte Carlo Methods in Practice, A. Doucet, J. F. G. de Freitas, and N. J. Gordon, Eds.*, New York: Springer-Verlag, 2001.

[39] E. Maggio and A. Cavallaro, "Hybrid particle filter and mean shift tracker with adaptive transition model", *Proc. IEEE Int. Conf. Acoustics, Speech, and Signal Processing*, 2005.

[40] A. Naeem, S. Mills, and T. Pridmore, "Structured combination of particle filter and kernel mean-shift tracking", *Proc. Int. Conf. Image and Vision Computing*, 2006.

[41] C. Shan, T. Tan, and Y. Wei, "Real-time hand tracking using a mean shift embedded particle filter", *Pattern Recognition*, vol. 40, no. 7, pp. 1958-1970, 2007.

[42] D.A. Zaugg, A.A. Samuel, D.E. Waagen, and H.A. Schmitt, "A combined particle/Kalman filter for improved tracking of beam aspect targets", *IEEE Statistical Signal Processing Workshop*, 2003.

[43] S.H. Won, W.W. Melek, and F. Golnaraghi, "A Kalman/particle filter-based position and orientation estimation method using a position sensor/inertial measurement unit hybrid system", *IEEE Trans. Ind. Electron.*, vol. 57, no. 5, pp. 1787-1798, 2010.

[44] R.J. Pawlak, "Combined unscented Kalman and particle filtering for tracking closely spaced objects", *IEEE Int. Conf. Information Fusion*, 2006.

[45] X. Xiang, "A brief review on visual tracking methods," *Chinese Conf. Intelligent Visual Surveillance (IVS)*, pp. 41-44, Dec. 2011.

[46] B. Babenko, M. Yang and S. Belongie, "Visual tracking with online multiple instance learning," *IEEE Conf. Computer Vision and Pattern Recognition (CVPR)*, pp. 983-990, Jun. 2009.

[47] J. Kwon and K. Lee, "Visual tracking decomposition," *IEEE Conf. Computer Vision and Pattern Recognition (CVPR)*, pp. 1269-1276, Jun. 2010.

[48] S. Avidan, "Ensemble tracking," *IEEE Trans. Pattern Anal. Mach. Intel.*, vol. 29, no. 2, pp. 261-271, Feb. 2007.

[49] D. Comaniciu, V. Ramesh, and P. Meer, "Real-time tracking of non-rigid objects using mean shift," *Proc. IEEE Conf. Computer Vision and Pattern Recognition*, vol. II, pp. 142-149, Jun. 2000.

[50] P. Perez, C. Hue, J. Vermaak, and M. Gangnet, "Color-based probabilistic tracking," *Proc. European Conf. Computer Vision*, vol. I, pp. 661-675, 2002.

[51] K. Nummiaro, E. Koller-Meier, and L. Van Gool, "Object tracking with an adaptive color-based particle filter," *Proc. 24th DAGM Symposium on Pattern Recognition*, pp. 353-360, 2002.

[52] K. Nummiaro, E. Koller-Meier, and L. Van Gool, "An adaptive color-based particle filter," *Image and Vision Computing*, vol. 21, pp. 99-110, 2003.

[53] F. Li, C. Li, and Z. Zhuang, "A hybrid object tracking method in complex backgrounds," *Proc. Int. Conf. Intelligent System and Knowledge Engineering*, pp. 1086-1091, 2008.

[54] T. Zhang, S. Fei, X. Li, and H. Lu, "An improved particle filter for tracking color object," *Int. Conf. Intelligent Computation Technology and Automation*, pp. 109-113, 2008.

[55] M. Fotouhi, A.R. Gholami, and S. Kasaei, "Particle filter-based object tracking using adaptive histogram," *Machine Vision and Image Processing (MVIP) 7th Iranian*, pp.1-5, Nov. 2011.

[56] Z. Wen and Y. Zhu, "A tracking algorithms based on particle filter using adaptive optimization," *Int. Conf. E-Product E-Service and E-Entertainment (ICEEE)*, pp. 1-4, Nov. 2010.

[57] J. Yang, X. Lu, H. Lu, and J. Wang, "An improved particle filter algorithm for target tracking," *Int. Conf. Intelligent Control, Automatic Detection and High-End Equipment (ICADE)*, pp. 103,107,27-29, 2012.

[58] J. Cheng, Y. Zhou, N. Cai, and J. Yang, "Infrared object tracking based on particle filters," *J. Infrared Millim. Waves*, vol. 25, no. 2, pp. 113-117, Apr. 2006.

[59] S. Chen and W. Huang, "Application of particle filter in target tracking from X-band nautical radar images," *IEEE NECEC Conference*, Newfoundland, Canada, 2012.

[60] S. Chen and W. Huang, "Target tracking using particle filter with X-band nautical radar," *Proc. IEEE Radar Conf. (RADAR)*, 2013.

[61] S. Chen and W. Huang, "Particle filter based maneuvering target tracking from nautical radar images," *Int. Conf. Remote Sensingand Wireless Communications (RSWC)*, 2014. (accepted)

[62] S. Chen and W. Huang, "Implementation of particle filter for target tracking using nautical radar," *IEEE NECEC Conference*, Newfoundland, Canada, 2013.

[63] S. Chen and W. Huang, "Maneuvering target tracking from nautical radar images using particle-Kalman filters," *J. Electromagnet. Wave and Applications*, vol. 27, no. 18, pp. 2366-2378, Nov. 2013.

[64] `http://www.radartutorial.eu/10.processing/sp20.en.html`

[65] G.L. Bair and E.D. Zink, "Radar track-while-scan methodologies," *IEEE Region 5 Conference: Spanning the Peaks of Electrotechnology*, pp. 32-37, Mar. 1988.

[66] P.M. Djuric, J.H. Kotecha, J. Zhang, Y. Huang, T. Ghirmai, M.F. Bugallo, and J. Miguez, "Particle filtering," *IEEE Signal Proces. Mag.*, vol. 20, no. 5, pp. 19-38, Sep. 2003.

[67] X.R. Li and V.P. Jilkov, "A survey of maneuvering target tracking-part IV: decision-based method," *SPIE Conf. Signal and Data Processing of Small Targets*, pp. 4728-4760, Apr. 2002.

[68] Y. Bar-Shalom and K. Birmiwal, "Variable dimension filter for maneuvering target tracking," *IEEE Trans. Aerosp. Electron. Syst.*, vol.AES-18, no. 5, pp. 621-629, Sep. 1982.

[69] A.H. Jazwinski, "Adaptive filtering," *Automatica*, vol. 5, pp. 475-485, 1969.

[70] H.A.P. Blom and Y. Bar-Shalom, "The interacting multiple model algorithm for systems with Markovian switching coefficients,", *IEEE Trans. Autom. Control*, vol. 33, no. 8, pp. 780-783, Aug. 1988.

[71] D. Comaniciu, V. Ramesh, and P. Meer, "Kernel-based object tracking," *IEEE Trans. Pattern Anal. Mach. Intell.*, vol. 25, no. 5, pp. 564-577, May 2003.

[72] T. Kailath, "The divergence and Bhattacharyya distance measures in signal selection," *IEEE Trans. Commun.*, vol. 15, no. 1, pp. 52-60, Feb. 1967.

[73] NMEA Reference Manual, SiRF Technology, Inc. November 2008, Revision 2.2, `http://www.usglobalsat.com/downloads/NMEA_commands.pdf`.

[74] R. G. Chamberlain, "GIS FAQ Q5.1: Great circle distance between 2 points", `http://www.movable-type.co.uk/scripts/gis-faq-5.1.html`.